Sellar and Parasellar Imaging

Carlos Zamora, MD, PhD

Mauricio Castillo, MD

Department of Radiology, Division of Neuroradiology, University of North Carolina School of Medicine, Chapel Hill, North Carolina

Correspondence:
Carlos Zamora, MD, PhD,
Division of Neuroradiology,
University of North Carolina School of Medicine,
3326 Old Infirmary Rd,
Chapel Hill, North Carolina 27514.
E-mail: carlos_zamora@med.unc.edu

The skull base is a complex anatomical region that harbors many important neurovascular structures in a relatively confined space. The pathology that can develop at this site is varied, and many disease processes may present with similar clinical and neuroimaging findings. While computed tomography maintains a role in the evaluation of many entities and can, for instance, delineate osseous erosion with great detail and characterize calcified tumor matrices, magnetic resonance imaging (MRI) is the mainstay in the neuroimaging assessment of most pathology occurring at the skull base. Various MRI sequences have proven to be robust tools for tissue characterization and can provide information on the presence of lipids, paramagnetic and diamagnetic elements, and tumor cellularity, among others. In addition, currently available MRI techniques are able to generate high spatial resolution images that allow visualization of cranial nerves and their involvement by adjacent pathology. The information obtained from such examinations may aid in the distinction of these disease processes and in the accurate delineation of their extent prior to biopsy or treatment planning.

KEY WORDS: Neuroimaging, Parasellar, Pituitary, Sella, Skull base, Sphenoid, Suprasellar

Characterization of sellar and parasellar lesions is challenging due to the anatomical complexity of the skull base, the extensive breadth of pathology that one may encounter, and the similar imaging appearance and clinical presentations of some entities. The presence of various critical neurovascular structures in a confined space complicates surgical access for tissue diagnosis or resection and underscores the importance of appropriate imaging. We review relevant neuroimaging aspects of sellar and parasellar lesions with particular attention to the anterior skull base.

RELEVANT ANATOMY AND EMBRYOLOGY

Pituitary Embryology

The adenohypophysis derives from a diverticulum that arises from the primitive oral cavity (Rathke's pouch) and projects toward the central skull base at around weeks 4 and 5.[1,2] A diencephalic infundibulum then projects inferiorly and contacts the diverticulum, which loses its connection to the oral cavity.[2] The anterior wall of the pouch fills with cells and forms the pars distalis, leaving a small cleft between it and the posterior wall, which becomes

the pars intermedia.[3] A small infundibular process grows superiorly and becomes the pars tuberalis.[2] The posterior diencephalic tissue evolves into the neurohypophysis.[4]

Anatomy of the Sphenoid Bone

The sphenoid bone is the largest component of the anterior skull base. Understanding its complex anatomy is key in evaluating sellar and parasellar pathology due to the popularity of endoscopic approaches to access many of these lesions.[5] The sphenoid bone holds the pituitary gland within the sella and adjacent structures, including cavernous sinuses and traversing cranial nerves. It features numerous foramina and fissures through which neurovascular structures pass. The sphenoid body is situated in the midline and has a cuboidal shape. Anterolaterally and superiorly, it extends as the greater wings forming the anteromedial aspects of the middle cranial fossae. The carotid sulci are located above their attachment to the sphenoid body lodging the internal carotid arteries and lateral cavernous sinuses. The lesser wings project posterolaterally, forming the superior orbital fissures between themselves and the greater wings. The flat surface connecting the lesser wings is the planum sphenoidale.

TABLE. Pituitary MRI Protocol at Our Institution	
Sequence	**Slice thickness (mm)**
Precontrast	
Sagittal T1	3
Axial T2	3
Coronal T1	3
Coronal T2	3
Postcontrast	
Coronal T1[a]	3
Coronal T1	3
Sagittal T1	3
Axial T1-MPRAGE	1

[a]Dynamic scan with 5 slices per acquisition every 30 s for 3 min.

The sella is a saddle-shaped concavity in the sphenoid body that is devoid of a bony covering laterally and superiorly. The pituitary gland is lodged in the sella and bounded laterally by cavernous sinuses, which are large venous plexuses between inner and outer layers of dura mater. The cavernous sinuses are interconnected via channels crossing the midline along the anterior, inferior, and posterior pituitary surfaces. A reflection of the inner dural layer above the pituitary gland forms the diaphragma sellae, which has a variable-sized opening for the infundibulum.

IMAGING PROTOCOLS

Magnetic resonance imaging (MRI) is a mainstay in the evaluation of sellar and parasellar pathology, due to intrinsic high-contrast resolution and availability of advanced sequences that offer high spatial resolution. Isotropic CISS (constructive interference in steady state) or its analog FIESTA-C (fast imaging employing steady-state acquisition cycled phases) are derived from steady-state free precession (SSFP) sequences that are acquired in a way that eliminates phase artifacts and generates fluid-sensitive images with high spatial resolution in a short period of time.[6] The isovolumetric data provide excellent contrast between fluid and surrounding tissues and can be reconstructed in any plane.[7] CISS and FIESTA-C are particularly useful for delineating the cisternal segments of the cranial nerves due to the bright signal from surrounding cerebrospinal fluid (CSF). Administration of intravenous contrast material in SSFP-based sequences allows visualization of the interdural cranial nerve segments and may be able to depict their relationship with skull base lesions.[8,9] High-resolution cranial nerve MRI should be performed at a minimum of 1.5 Tesla and ideally at 3.0 Tesla, as the latter provides higher signal-to-noise ratio and increases the conspicuity of cranial nerves.[10] Isovolumetric gradient echo T1-weighted MR sequences (volumetric interpolated brain examination, VIBE, or magnetization-prepared rapid acquisition with gradient echo, MP-RAGE) allow for multiplanar reconstructions. However, contrast enhancement may be less conspicuous compared to spin-echo images.[11]

For the pituitary gland, thinner slices are acquired with smaller field of views centered at the sella. Dynamic contrast-enhanced sequences are obtained in the coronal plane and acquired every 30 s for 3 min following intravenous contrast injection (Table). These take advantage of the different contrast dynamics of adenomas in relation to pituitary tissue and may be useful for evaluation of small tumors.[12,13] Most adenomas enhance more slowly (peak between 60 and 200 s) than the briskly and avidly enhancing pituitary tissue.[14]
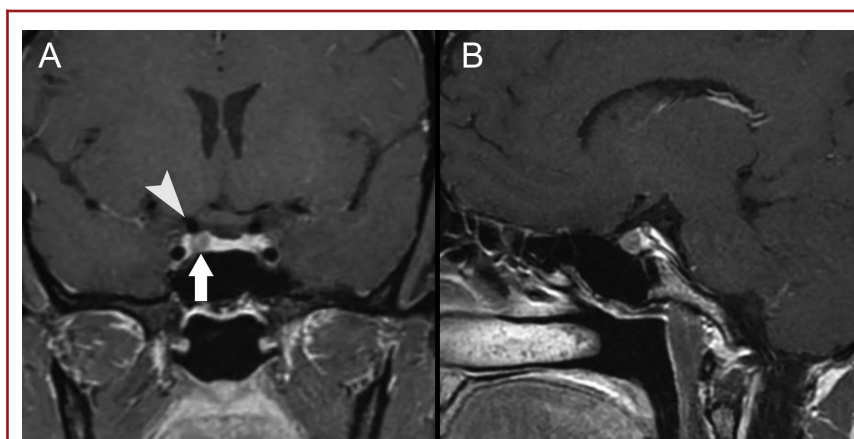
FIGURE 1. *Microadenoma.* **A**, *Coronal and* **B** *sagittal postcontrast T1-weighted images demonstrate a small hypoenhancing focus in the right pituitary gland (arrow, A) abutting the right supraclinoid internal carotid artery (arrowhead, A). Notice upward convexity of the right superior pituitary surface and slight bulging into the suprasellar cistern without compression of the optic chiasm or nerves.*
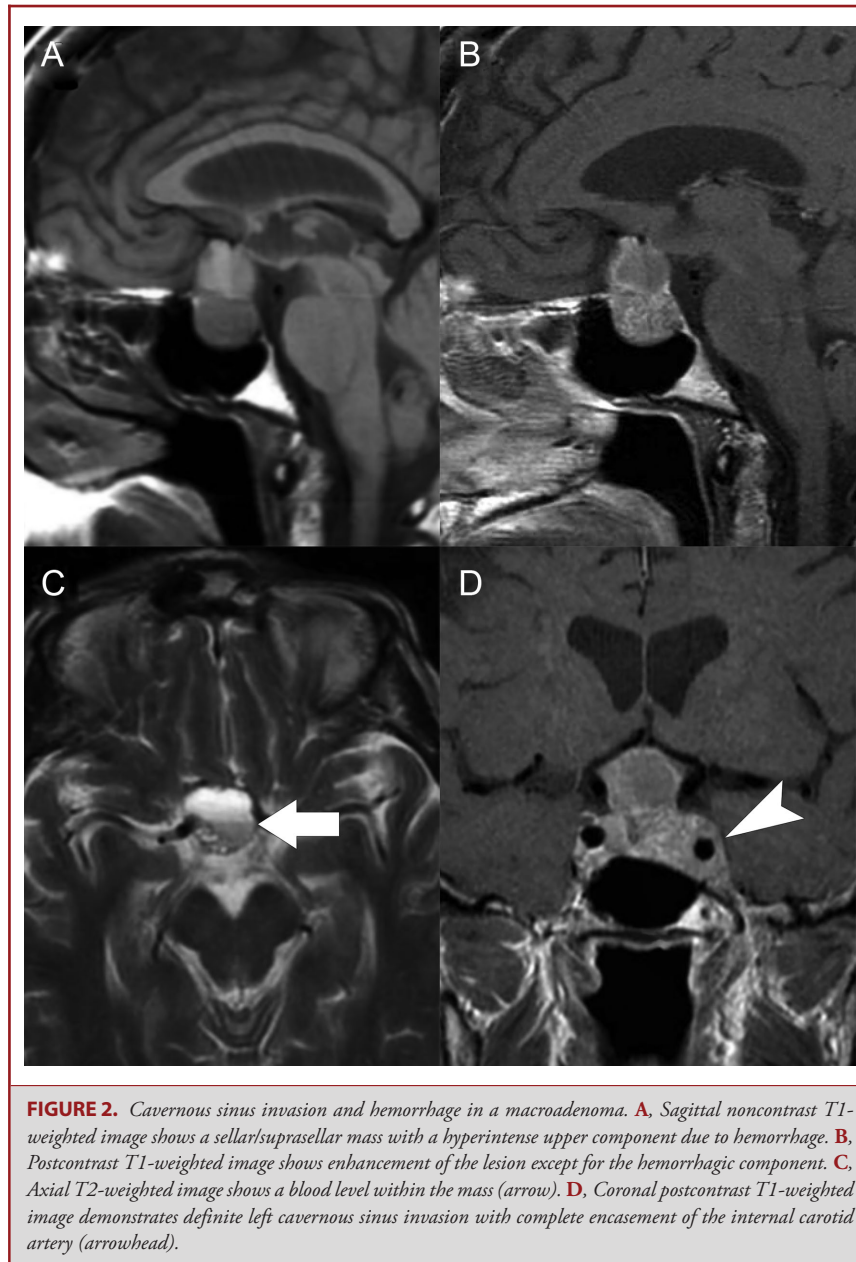
FIGURE 2. *Cavernous sinus invasion and hemorrhage in a macroadenoma.* **A**, *Sagittal noncontrast T1-weighted image shows a sellar/suprasellar mass with a hyperintense upper component due to hemorrhage.* **B**, *Postcontrast T1-weighted image shows enhancement of the lesion except for the hemorrhagic component.* **C**, *Axial T2-weighted image shows a blood level within the mass (arrow).* **D**, *Coronal postcontrast T1-weighted image demonstrates definite left cavernous sinus invasion with complete encasement of the internal carotid artery (arrowhead).*

NEOPLASTIC

Pituitary Adenoma

Adenomas account for 10% to 15% of intracranial tumors.[15] They have a prevalence of 17% based on a meta-analysis of autopsy and imaging data.[16] Adenomas have been arbitrarily classified into microadenomas (<10 mm) and macroadenomas (≥10 mm). Microadenomas may be difficult to detect due to their size but nonetheless be highly symptomatic, while macroadenomas have the potential to exert mass effect. Adenomas can also be classified according to their cellular origin into lactotrophs, somatotrophs, gonadotrophs, corticotrophs, and thyrotrophs. In an epidemiologic study, 74% of macroadenomas and 22% of microadenomas were nonfunctioning.[17] Functioning adenomas secrete prolactin in 25% to 41% and adrenocorticotropic and growth hormones in 5% and 2.8% of cases, respectively.[16]

Identification of small lesions may benefit from dynamic contrast-enhanced MRI or, rarely, computed tomography (CT) techniques (usually when MRI cannot be performed) based on the differential rate of enhancement of adenomas compared to

FIGURE 3. *Giant invasive macroadenoma.* **A**, *Axial postcontrast T1-weighted image shows tumor invading the cavernous sinuses, sinonasal cavity, right orbit, and left middle cranial fossa.* **B**, *Coronal postcontrast T1-weighted image shows carotid encasement bilaterally and mass effect on the right prechiasmatic optic nerve.*
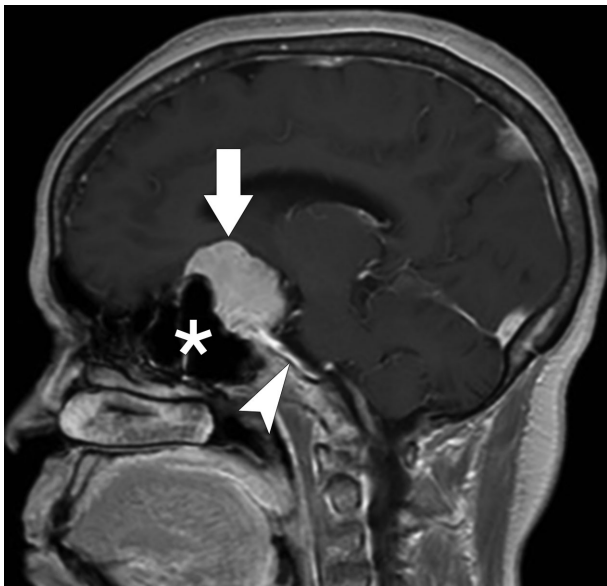
FIGURE 4. *Meningioma. Sagittal postcontrast T1-weighted image shows an avidly enhancing meningioma along the planum sphenoidale, tuberculum sellae, and sella turcica (arrow) with an associated dural tail (arrowhead) and pneumosinus dilatans (star).*
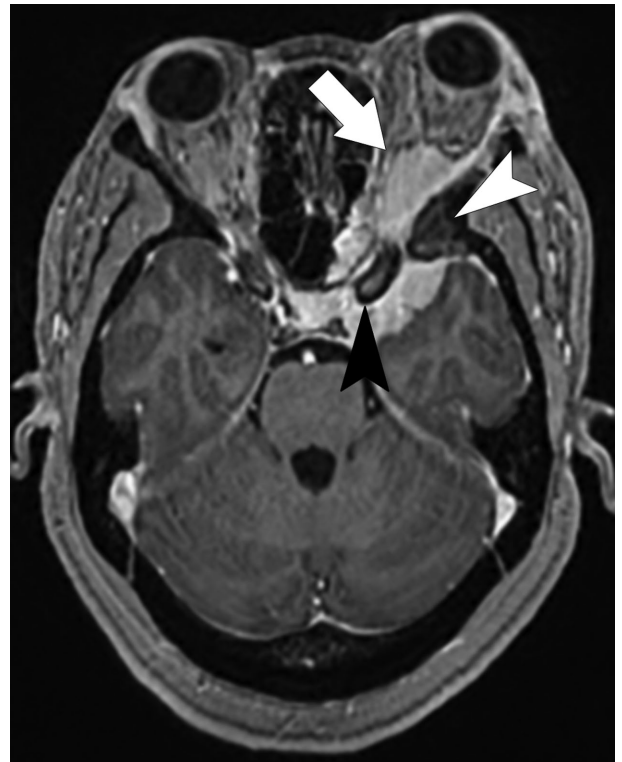

FIGURE 5. *Meningioma. Axial postcontrast T1-weighted image demonstrates a meningioma invading the left orbit (arrow) and posterior ethmoid cells. Note hyperostosis of the greater sphenoid wing (white arrowhead) and anterior clinoid process (black arrowhead).*
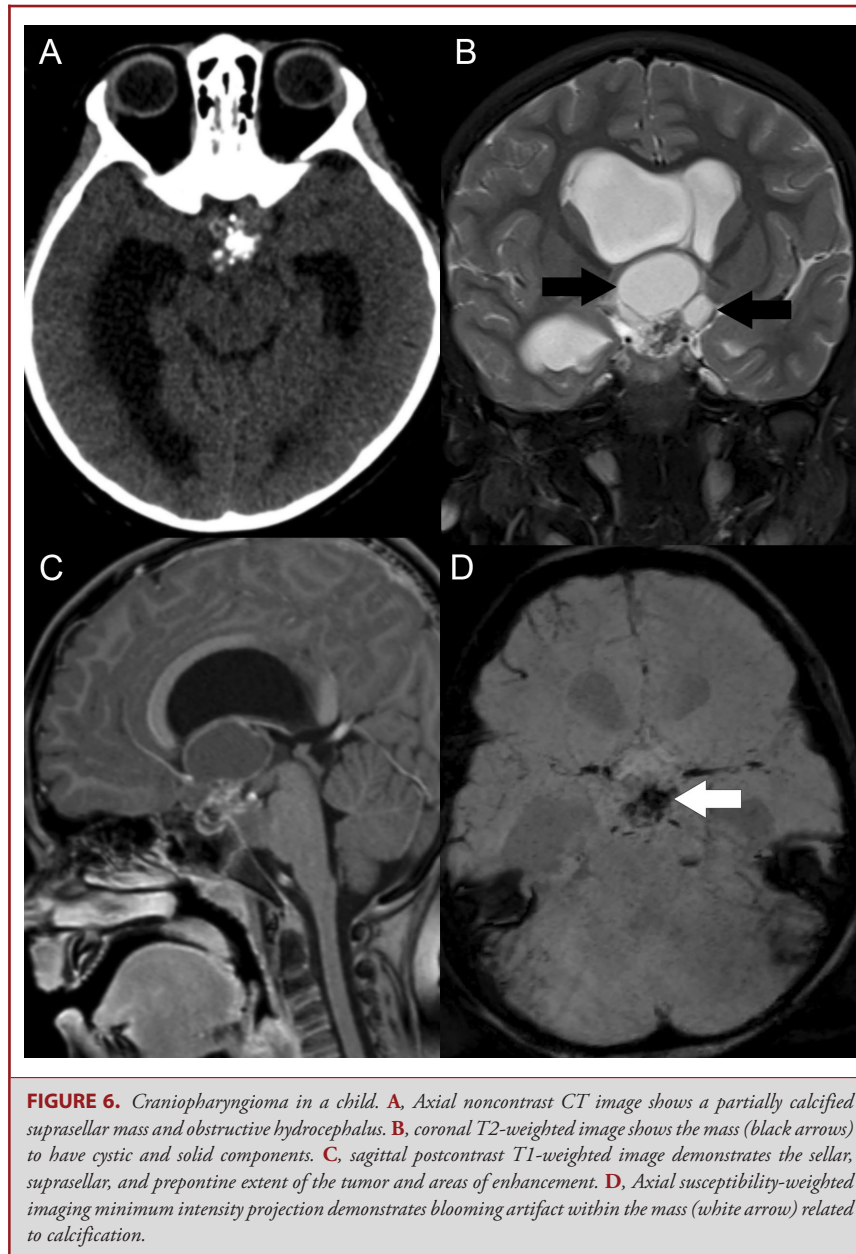
FIGURE 6. *Craniopharyngioma in a child.* **A**, *Axial noncontrast CT image shows a partially calcified suprasellar mass and obstructive hydrocephalus.* **B**, *coronal T2-weighted image shows the mass (black arrows) to have cystic and solid components.* **C**, *sagittal postcontrast T1-weighted image demonstrates the sellar, suprasellar, and prepontine extent of the tumor and areas of enhancement.* **D**, *Axial susceptibility-weighted imaging minimum intensity projection demonstrates blooming artifact within the mass (white arrow) related to calcification.*

pituitary tissue. Normal pituitary parenchyma shows homogeneous enhancement at 60 to 80 s following administration of contrast material.[18] Maximum image contrast between adenomas and pituitary tissue occurs at about 1 min and gradually decreases thereafter (Figure 1).[19] However, an adenoma may enhance earlier than pituitary tissue due to direct arterial supply.[18] While signal intensity on T2-weighted sequences is variable (particularly in large tumors) due to hemorrhage, cysts, or necrosis,[20] T2 hypointensity has been commonly reported in growth-hormone-producing adenomas.[21,22]

Large adenomas usually infiltrate the gland; therefore, a displaced but otherwise normal-appearing pituitary gland may be helpful in ruling out an adenoma. Up to 10% of adenomas invade the cavernous sinuses (more frequently larger lesions) and tend to be biologically aggressive, with increased surgical morbidity and mortality.[22-24] Imaging features that may be indicative or highly suggestive of cavernous sinus invasion (or absence of such) are usually assessed on coronal pre- and postcontrast T1-weighted sequences.[24,25] In one study, greater than 67% encasement of the internal carotid artery by tumor (about 241°) yielded a
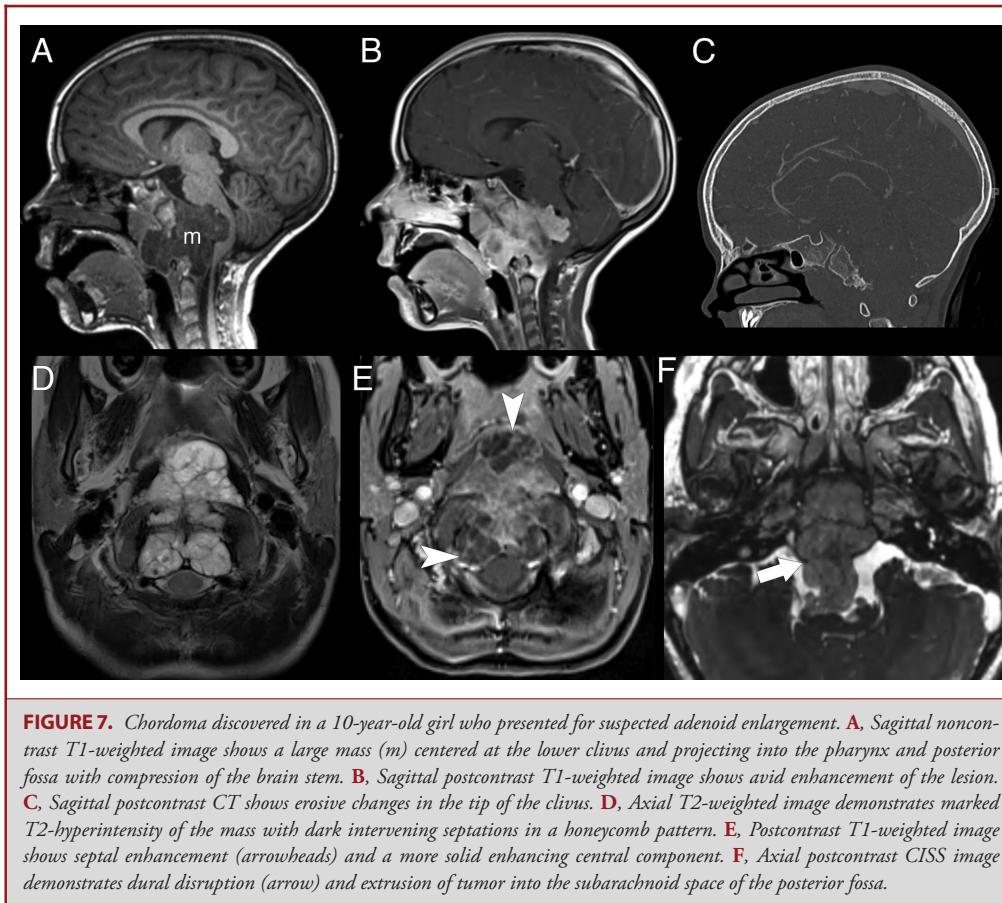
FIGURE 7. *Chordoma discovered in a 10-year-old girl who presented for suspected adenoid enlargement.* **A***, Sagittal noncontrast T1-weighted image shows a large mass (m) centered at the lower clivus and projecting into the pharynx and posterior fossa with compression of the brain stem.* **B***, Sagittal postcontrast T1-weighted image shows avid enhancement of the lesion.* **C***, Sagittal postcontrast CT shows erosive changes in the tip of the clivus.* **D***, Axial T2-weighted image demonstrates marked T2-hyperintensity of the mass with dark intervening septations in a honeycomb pattern.* **E***, Postcontrast T1-weighted image shows septal enhancement (arrowheads) and a more solid enhancing central component.* **F***, Axial postcontrast CISS image demonstrates dural disruption (arrow) and extrusion of tumor into the subarachnoid space of the posterior fossa.*

100% positive predictive value (PPV) for invasion as confirmed by surgery.[24] Other imaging findings included obliteration of the carotid sulcus venous compartment (95% PPV) and tumor extension beyond the lateral intercarotid line (85% PPV).[24] Features predicting absence of invasion include less than 25% of carotid encasement, presence of pituitary tissue between the tumor and carotid artery, and tumor not extending beyond the medial intercarotid line (Figure 2).[24]

Five percent to 14% of surgically treated adenomas are classified as "giant" (greater than 4 cm).[15] Despite their benign histology, such tumors can infiltrate the skull base and, rarely, extend to the nasopharynx (Figure 3).[26] Large adenomas undergo spontaneous infarction at a greater rate than any other central nervous system (CNS) tumor, probably due to outgrowth of their blood supply, vascular compression from expansion, or other intrinsic features.[27,28] This occurs with or without hemorrhage and may lead to pituitary apoplexy, which can rarely be complicated by retroclival hematomas.[27,29] Pituitary carcinomas are exceedingly rare, and distant spread is the only imaging feature that may distinguish them from adenomas.[30]

Meningioma

Meningiomas constitute the most common primary CNS neoplasms, with an incidence of 7 in 100 000 individuals according to one population-based study.[31] They are 3 times more common in females and are largely tumors of adulthood, with greater than 70% occurring after age 55.[31] Meningiomas are rarely seen in children unless syndromic or associated with radiation (less than 2% occur in patients 20 yr of age or younger).[32] With 15 subtypes in the 2007 WHO classification, they are histologically heterogeneous, although most (90%) are benign and classified as grade I.[33] Six percent of meningiomas are anaplastic (grade II) and 5% frankly malignant (grade III).[33] Meningiomas arise from arachnoid cap cells in the leptomeninges, which derive from the mesenchyme and neural crest.[34,35] They are almost always dural-based (but may be intraventricular or very rarely extracranial) and commonly occur along dural reflections. Approximately 40% arise in the skull base.[36] Roughly one-half of anterior skull base meningiomas arise at the sphenoid wings and the remainder from the tuberculum sellae, limbus sphenoidale, and
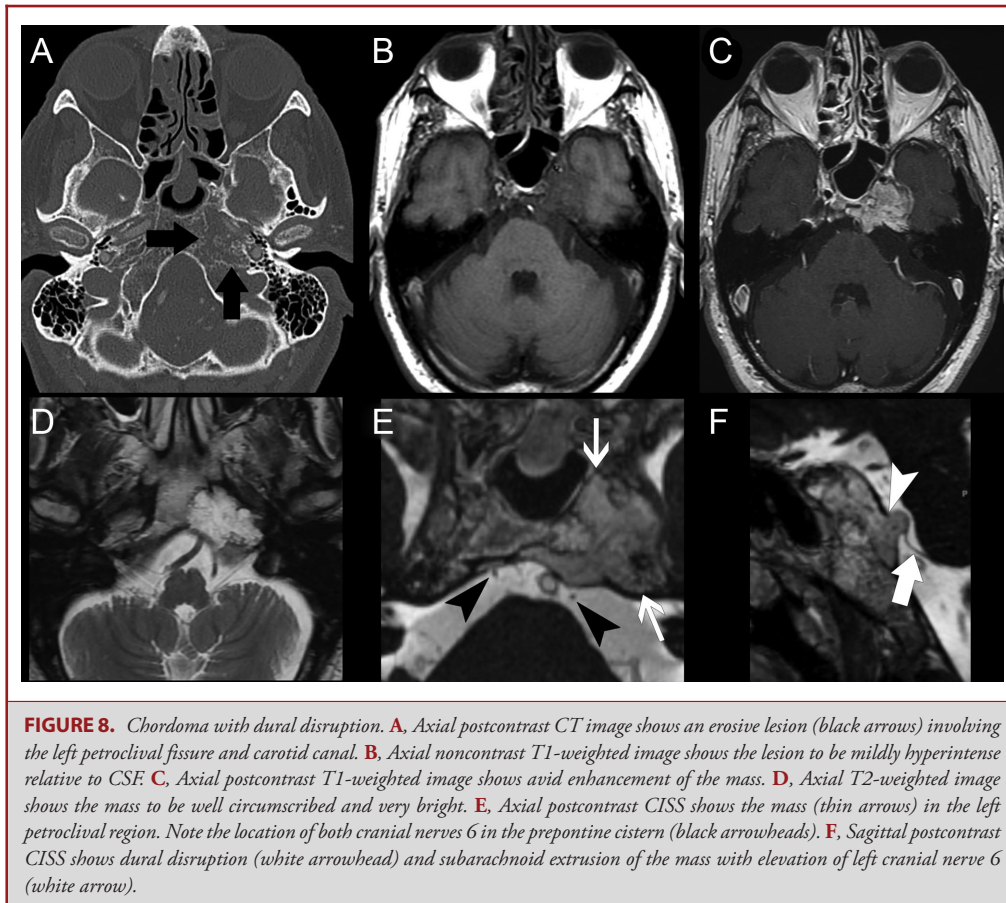
FIGURE 8. *Chordoma with dural disruption.* **A**, *Axial postcontrast CT image shows an erosive lesion (black arrows) involving the left petroclival fissure and carotid canal.* **B**, *Axial noncontrast T1-weighted image shows the lesion to be mildly hyperintense relative to CSF.* **C**, *Axial postcontrast T1-weighted image shows avid enhancement of the mass.* **D**, *Axial T2-weighted image shows the mass to be well circumscribed and very bright.* **E**, *Axial postcontrast CISS shows the mass (thin arrows) in the left petroclival region. Note the location of both cranial nerves 6 in the prepontine cistern (black arrowheads).* **F**, *Sagittal postcontrast CISS shows dural disruption (white arrowhead) and subarachnoid extrusion of the mass with elevation of left cranial nerve 6 (white arrow).*

chiasmatic and olfactory grooves (Figure 4).[37] Therefore, extension frequently occurs into the optic canals, cavernous sinuses, or sella (Figure 5). Arterial encasement may be present, which can lead to stenosis.[38] Anterior skull base meningiomas can result in abnormal dilatation of an adjacent paranasal sinus (pneumosinus dilatans).[39]

On noncontrast CT, meningiomas tend to be iso- to hyperdense to cerebral cortex and are difficult to visualize unless they are large or calcified or there is hyperostosis, which appears to be more common in the skull base (occurring in 50% of patients) compared to convexity meningiomas.[40] On MRI they are usually well circumscribed, iso- to hypointense on T2, and show avid contrast enhancement, although this will vary according to the degree of calcification or, rarely, cystic degeneration. Although not entirely specific, identification of a dural tail may suggest a meningioma if the original definition is applied: the tail must (a) be thicker closer to the tumor and taper peripherally, (b) enhance to a greater degree than the tumor, and (c) be seen in 2 consecutive tumor sections and more than one plane.[41,42] Studies on their apparent diffusion coefficient (ADC) characteristics have yielded variable results.[43]

Craniopharyngioma

Craniopharyngiomas are nonglial epithelial tumors arising from remnants of Rathke's pouch or rests of buccal mucosa at any point along the trajectory of the craniopharyngeal duct.[44] While their most common site of origin is the infundibulum, where squamous epithelial rests are known to occur, they may rarely arise primarily within the third ventricle, sphenoid bone, or even nasopharynx.[45] They are rare, with an incidence of 0.5 to 2 cases per million persons per year, up to half occurring during childhood and adolescence.[46] They constitute 4% of intracranial neoplasms in the pediatric population and have a bimodal distribution, with peaks at 5 to 14 and 50 to 75 yr of age.[47,48] Histologically, craniopharyngiomas are almost always benign and have a high survival rate, but they can be locally aggressive and may be associated with significant morbidity.[46] Those occurring in childhood are more commonly of the adamantinomatous type and present as heterogeneous cystic and solid suprasellar masses (Figure 6). Approximately 90% of these have calcifications that can be readily identified on CT.[44,46] The solid portions show contrast enhancement, and on MRI the cystic
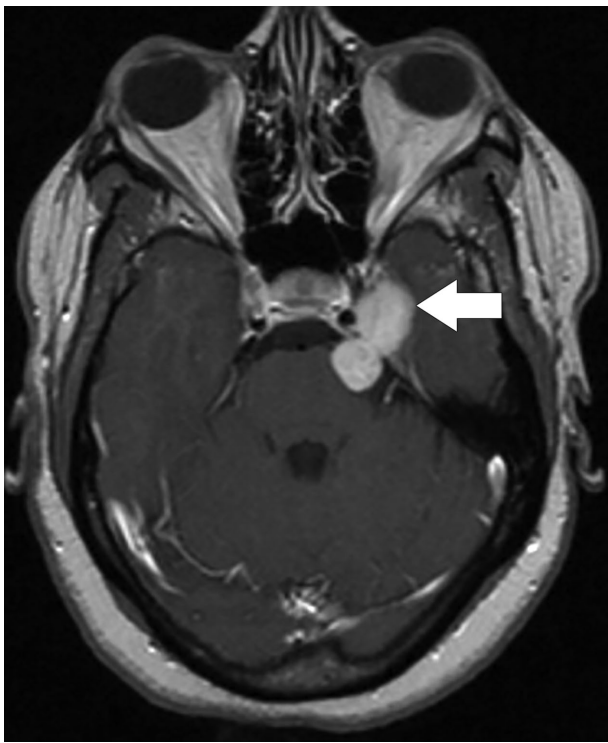
FIGURE 9. *Trigeminal schwannoma. Axial postcontrast T1-weighted image shows an avidly enhancing schwannoma (arrow) involving the trigeminal ganglion within Meckel cave and the cisternal segment of the nerve.*

components may present with variable signal intensities depending on their contents of protein, cholesterol, or hemorrhage.[44] Tumors in adulthood are more commonly of the papillary type and are solid, less commonly calcified, and devoid of cysts.[44,46] Due to their preferred infundibular location, age at presentation, and solid appearance with lack of calcification or cystic changes, papillary craniopharyngiomas may be difficult to distinguish from germinomas. While they both usually show strong contrast enhancement, germinomas have lower ADC values by virtue of their higher grade histology and cellularity compared to papillary craniopharyngiomas.[49]

Chordoma

Most chordomas are histologically low-grade but locally aggressive tumors derived from embryonic remnants of the notochord.[50] Three subtypes have been recognized, with the conventional form accounting for the majority, followed by chondroid chordoma with cartilaginous elements and the rare dedifferentiated chordomas, which are malignant and have the worst prognosis.[51,52] Half of all chordomas are sacrococcygeal, one-third occur in the skull base, and a minority arise in the spine.[51] They are twice as common in males, have a peak incidence between 50 and 60 yr of age, and are rare in children and adolescents.[52] These tumors most frequently occur midline at the spheno-occipital synchondrosis, although the chondroid subtype has a tendency to arise laterally at the petroclival junction.[50,53] Chordomas are extradural and almost always originate in bone, which may lead to bony sequestra (the chondroid variant may have a true calcific matrix) that can be demonstrated on CT.[53] On MRI, chordomas are well circumscribed with a pseudoencapsulated appearance and markedly bright on T2-weighted sequences, probably secondary to mucin and/or necrosis.[53] T2 signal in the chondroid variant may be relatively low due to cartilaginous tissue.[54] Interlobular septa are formed by epithelioid cells and appear hypointense on T2 with variable degrees of contrast enhancement (Figure 7).[53] Chordomas are soft tumors that tend to displace or encase blood vessels, but stenoses are rare.[55] Dural transgression can be present, and tumor can extend
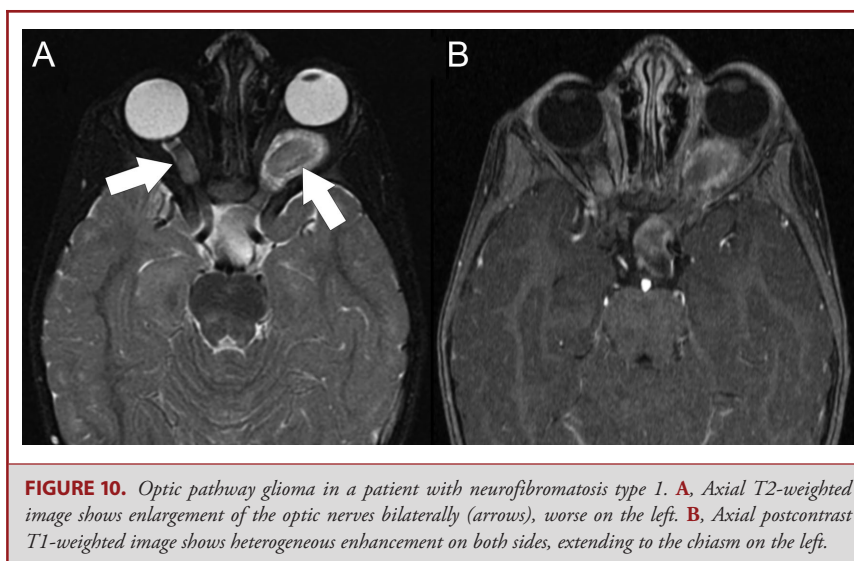
FIGURE 10. *Optic pathway glioma in a patient with neurofibromatosis type 1.* **A**, *Axial T2-weighted image shows enlargement of the optic nerves bilaterally (arrows), worse on the left.* **B**, *Axial postcontrast T1-weighted image shows heterogeneous enhancement on both sides, extending to the chiasm on the left.*
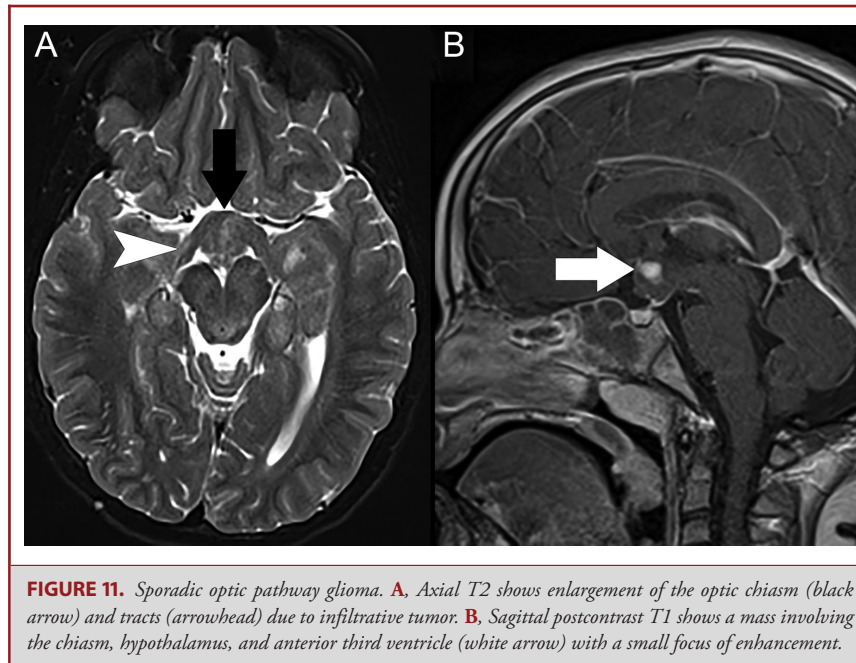
FIGURE 11. *Sporadic optic pathway glioma. **A**, Axial T2 shows enlargement of the optic chiasm (black arrow) and tracts (arrowhead) due to infiltrative tumor. **B**, Sagittal postcontrast T1 shows a mass involving the chiasm, hypothalamus, and anterior third ventricle (white arrow) with a small focus of enhancement.*
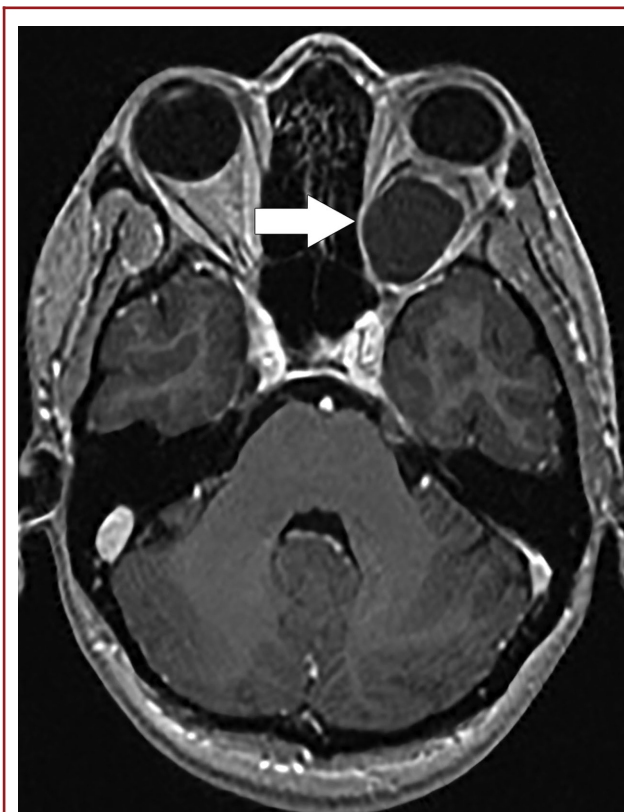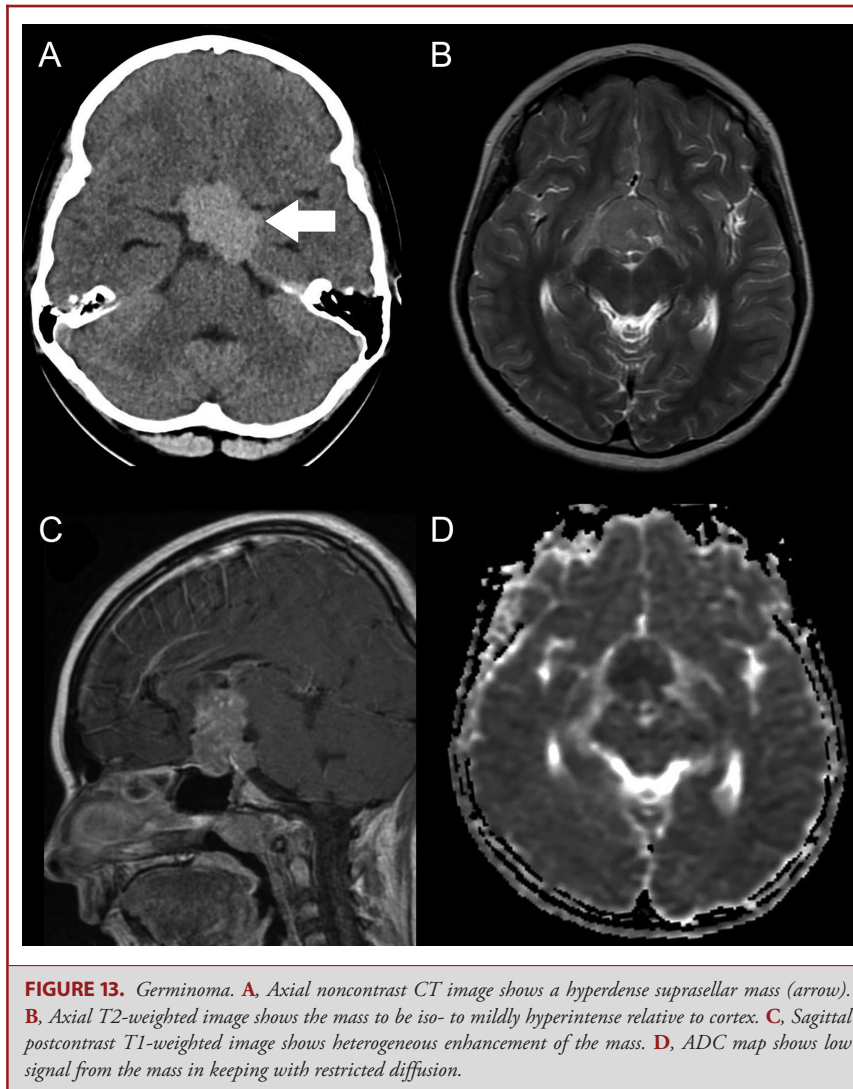

FIGURE 12. *Cystic optic pathway glioma. Axial postcontrast T1-weighted image shows a nonenhancing cystic mass (arrow) expanding the left optic nerve.*

into the subarachnoid space, increasing the risk of CSF leaks and infection.[56] Dural disruption may be identified on T2-weighted imaging but is best visualized on high-resolution SSFP-based sequences, where administration of contrast may aid in delineation of tumor against nonenhancing dura and depiction of its relationship to cranial nerves (Figure 7).[8]

Chondrosarcoma

Chondrosarcomas are often described together with chordomas, as they share similar imaging features, clinical presentations, and locations. Both are rare and usually present in adults between the fourth and fifth decades of life and together constitute less than 1% of intracranial tumors.[50,57] Chondrosarcomas represent 6% of all skull base tumors, and only 1% of them occur at this site.[58] Compared to chordomas, conventional chondrosarcomas are relatively indolent and have a more favorable prognosis.[50] Metastases and recurrence are rare, except for the unusual dedifferentiated subtype, which has an aggressive course.[59] While pathogenesis is uncertain, chondrosarcomas are believed to arise from chondrocytes within endochondral cartilage rests and are commonly located at the petroclival (two-third of cases), spheno-occipital, and sphenopetrosal synchondroses, therefore more commonly off-midline compared to chordomas.[60,61] CT demonstrates osseous erosions and destructive changes usually with a calcified chondroid matrix that may have typical "rings and arcs" or nonspecific foci of amorphous calcifications.[62] Similarly, on MRI, chondrosarcomas are usually well circumscribed and hyperintense on T2-weighted sequences, with variable degrees of heterogeneous contrast enhancement (Figure 8).[50,57,61] As opposed to chordomas,

FIGURE 13. *Germinoma.* **A**, *Axial noncontrast CT image shows a hyperdense suprasellar mass (arrow).* **B**, *Axial T2-weighted image shows the mass to be iso- to mildly hyperintense relative to cortex.* **C**, *Sagittal postcontrast T1-weighted image shows heterogeneous enhancement of the mass.* **D**, *ADC map shows low signal from the mass in keeping with restricted diffusion.*

chondrosarcomas more often present with ophthalmoplegia, presumably due to their preferred lateral location.[61] Finally, while some of their imaging features overlap, a recent study using diffusion-weighted imaging suggests that chondrosarcomas have significantly higher ADC values than chordomas.[63]

Schwannoma

Schwannomas are benign, slow-growing neoplasms that arise from Schwann cells. They make up 8.5% of intracranial tumors and are usually seen in adulthood, the overwhelming majority originating from cranial nerve (CN) VIII (90%), followed by CN V (1%-8%) and CN VII.[64] In the parasellar region, CN V schwannomas predominate, while CN III, IV, and VI schwannomas are rare, except in the setting of neurofi-

bromatosis type 2.[64] The most common location of CN V schwannomas is the gasserian ganglion, but they can also affect the cisternal or postganglionic segments, and the cavernous sinus is often involved.[65,66] Most patients present with CN V dysfunction, although symptoms related to compression of CN VI within Dorello's canal may be present.[65] On MRI, schwannomas are iso- to hypointense on T1 and hyperintense on T2-weighted sequences and show avid contrast enhancement (Figure 9).[65,67] Their heterogeneity varies according to the presence of cystic changes or, rarely, hemorrhage or calcifications.[65-67] Melanotic schwannomas are rare and show intrinsic T1 hyperintensity, in which case they may be confused with lipomas, although the latter suppress on fat-saturated sequences.[59,68,69]
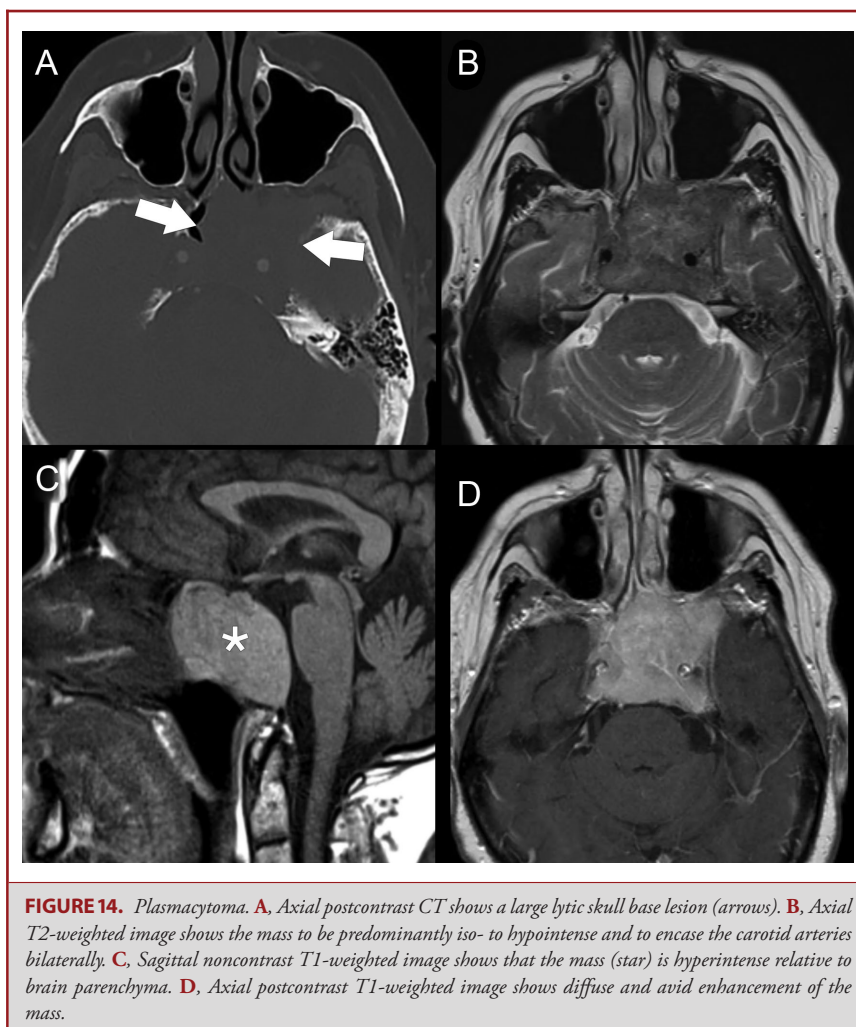
FIGURE 14. *Plasmacytoma.* **A**, *Axial postcontrast CT shows a large lytic skull base lesion (arrows).* **B**, *Axial T2-weighted image shows the mass to be predominantly iso- to hypointense and to encase the carotid arteries bilaterally.* **C**, *Sagittal noncontrast T1-weighted image shows that the mass (star) is hyperintense relative to brain parenchyma.* **D**, *Axial postcontrast T1-weighted image shows diffuse and avid enhancement of the mass.*
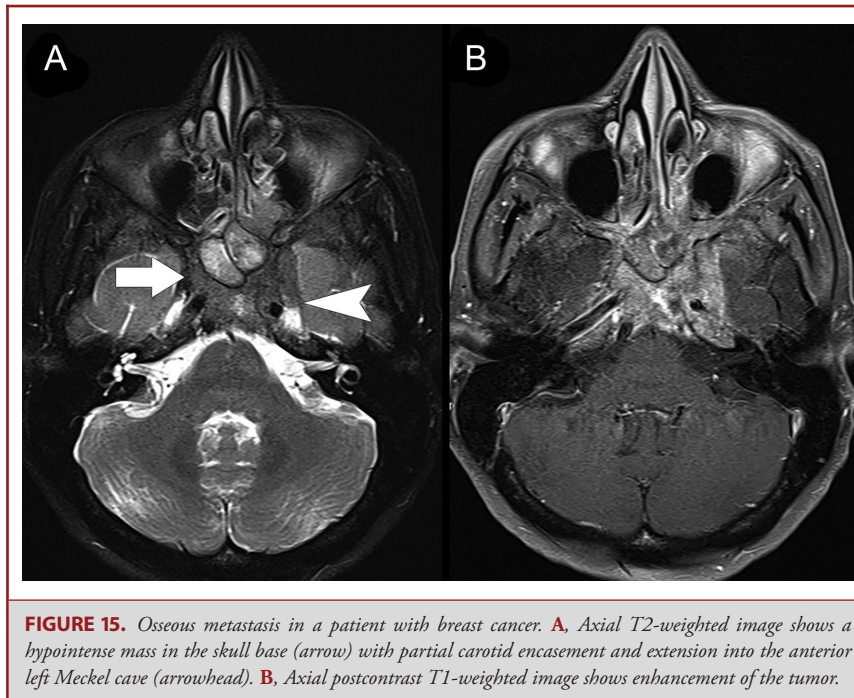
Optic Pathway Glioma

These lesions represent 3% to 5% of brain tumors in children, and the great majority are diagnosed before age 20.[70] They account for 65% of all optic nerve tumors, and roughly one-third are associated with neurofibromatosis type 1.[71] They are, in fact, the most common CNS neoplasms in this syndrome, in which they have been reported in 7% to 20% of children.[70] Syndromic optic nerve gliomas almost always develop before age 4 and are low grade and generally indolent.[72] While it appears that sporadic gliomas are associated with worse outcomes, their presentation differs from syndromic tumors in that the latter are usually found in asymptomatic patients as part of routine screening and their natural history has not been conclusively demonstrated.[73] Syndromic status also has implications for tumor location. Optic pathway gliomas in neurofibromatosis type 1 more frequently involve the optic nerves, while sporadic ones favor a chias-

matic or postchiasmatic location (Figures 10 and 11).[72,73] On MRI, they infiltrate and cause enlargement of optic nerves, chiasm, and/or optic tracts. They are iso- to hypointense on T1 and hyperintense on T2-weighted sequences and usually well demarcated.[73] Enhancement is variable and does not correlate with tumor grade.[74] Calcifications are uncommon and hemorrhage is exceedingly rare.[70,72,75] Cysts may be present and are more common in sporadic tumors (Figure 12).[72] Increased T2 signal is generally not useful to evaluate involvement of the optic tracts, as it may be also related to edema.[72] Postcontrast images may be helpful in this regard, since enhancement indicates tumor.[74]

Germ Cell Tumor

Germinomas represent 50% to 70% of intracranial germ cell tumors, with the rest belonging to the nongerminomatous

FIGURE 15. *Osseous metastasis in a patient with breast cancer.* **A**, *Axial T2-weighted image shows a hypointense mass in the skull base (arrow) with partial carotid encasement and extension into the anterior left Meckel cave (arrowhead).* **B**, *Axial postcontrast T1-weighted image shows enhancement of the tumor.*

FIGURE 16. *Rathke cleft cyst. Sagittal noncontrast T1-weighted image shows a hyperintense cyst (arrow) displacing the pars distalis anteriorly. Note the thin pars intermedia between the cyst and the bright posterior pituitary (arrowhead).*

subtype.[76] Germ cell tumors are predominantly seen in children and account for nearly 4% of pediatric intracranial tumors in the United States, most of them diagnosed between 5 and 14 yr of age.[48] Pure germinomas are usually diagnosed in patients between 10 and 21 yr of age, while nongerminomatous tumors are more often seen in younger children.[76] The incidence of intracranial germ cell tumors is significantly higher in Asian countries and also in patients of Asian descent living in the United States.[77] Alfa-fetoprotein and β-human chorionic gonadotropin are commonly found in CSF and serum and may be helpful markers for diagnosis.[76,78]

Intracranial germ cell tumors favor a midline location around the third ventricle.[79] The majority of lesions arising in the pineal region are nongerminomatous, while suprasellar ones are more likely to be germinomas, with these 2 sites constituting the most common locations.[80] Five percent to 10% of germinomas are ectopic and occur in basal ganglia or thalami.[81] These have an increased incidence in Asia and may be associated with ipsilateral cerebral or brainstem atrophy.[82] Rarely, germinomas may occur within the sella turcica.[30] While pineal germ cell tumors are most common in males, suprasellar ones are slightly more frequent in females.[30,78] Pure germinomas are exquisitely radiosensitive, with survival rates greater than 90% at 5 yr with radiotherapy alone.[76]

The earliest finding of a suprasellar germinoma may be absence of the pituitary bright spot due to disruption of the infundibulo-neurohypophyseal system.[30] Enhancement is typically avid and
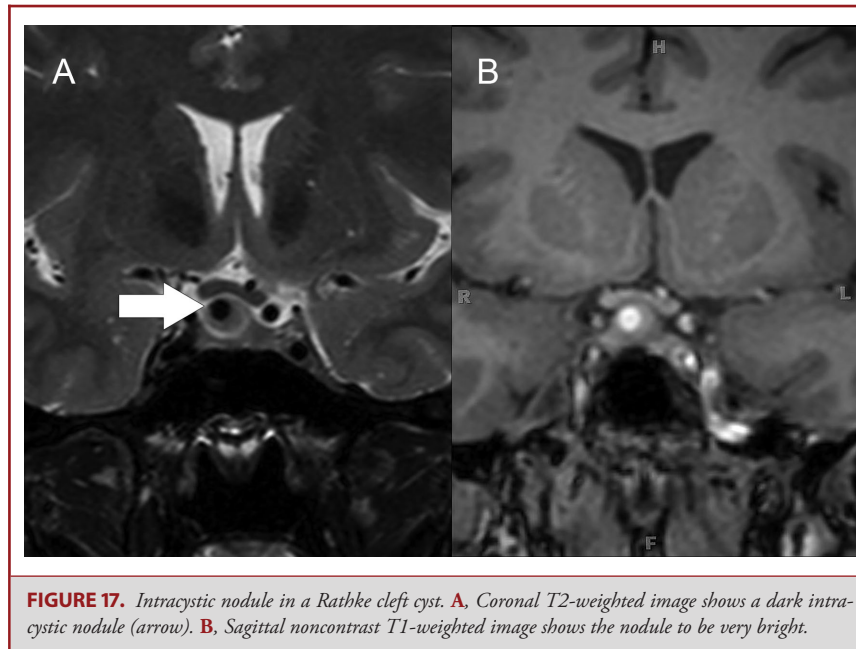
FIGURE 17. *Intracystic nodule in a Rathke cleft cyst.* **A**, *Coronal T2-weighted image shows a dark intra-cystic nodule (arrow).* **B**, *Sagittal noncontrast T1-weighted image shows the nodule to be very bright.*

more homogeneous in germinomas compared to nongermi-nomatous tumors, which are more commonly hemorrhagic.[83] Germinomas are highly cellular and, as a result, show restricted diffusion on MRI and are usually hyperdense on CT.[83,84] Compared to nongerminomatous tumors, one study suggests that germinomas may show lower ADC values on MRI (Figure 13).[85] However, conventional imaging characteristics of germinomas and nongerminomatous tumors are similar, and reliable discrimi-nation between histologic subtypes is not possible.[76] These lesions are iso- to slightly hyperintense on T2-weighted images, and T1 signal intensity is variable.[83,84] Cystic changes may be seen, and calcifications are unusual (as opposed to pineal region tumors, in which calcifications may "engulf" the pineal gland).[84] Germ cell tumors have a high propensity to seed CSF, and therefore imaging of the entire neuraxis is warranted.[30]
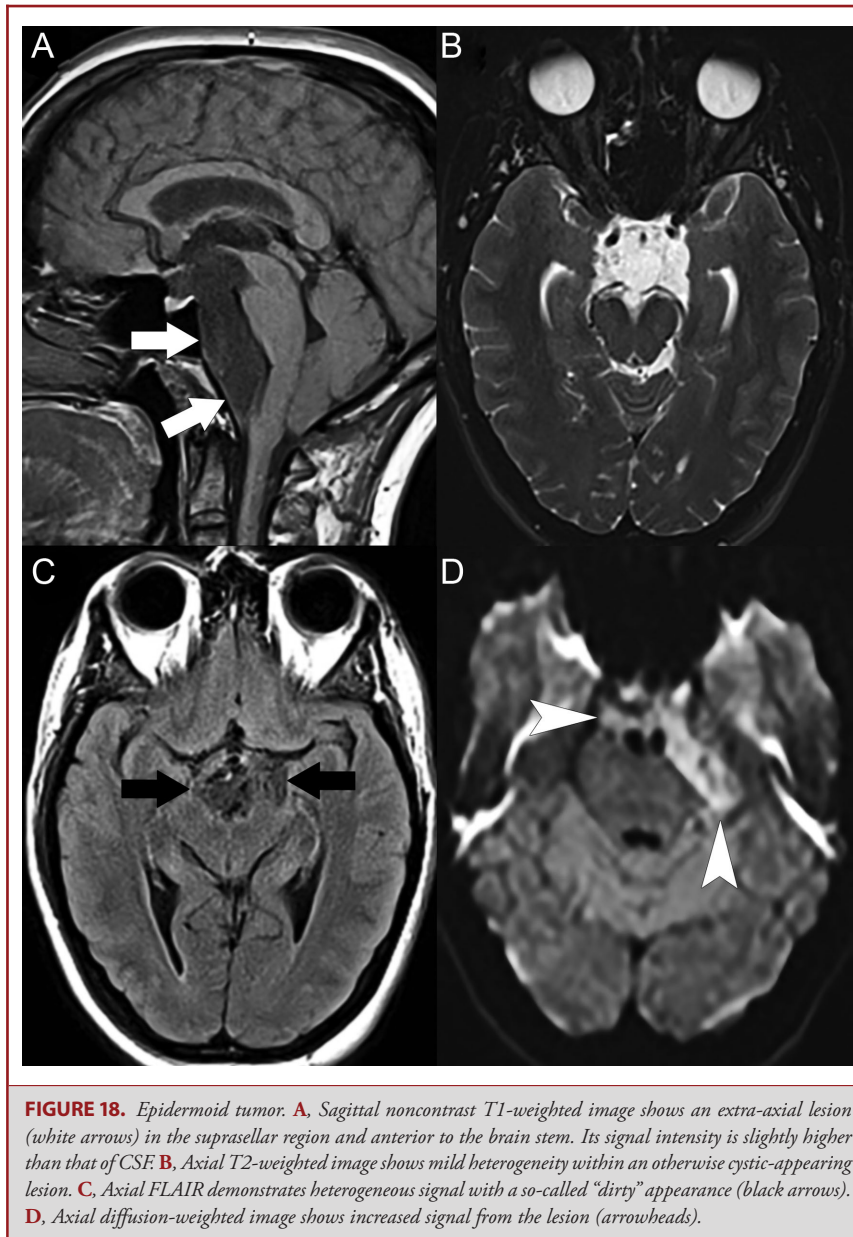
Plasmacytoma

Plasma cell neoplasms can present systemically as multiple myeloma or as discrete masses in the form of plasmacytomas.[86] Plasmacytomas are usually intramedullary and solitary but may occasionally be multiple or extramedullary.[86] By definition, solitary plasmacytomas occur without other stigmata of multiple myeloma, such as anemia, renal insufficiency, or scattered skeletal lesions.[87] Skull base plasmacytomas usually arise from the nasopharynx, clivus, or petrous apex.[88] The great majority of patients with a solitary plasmacytoma will develop multiple myeloma, although this appears to be less common with extramedullary tumors.[88,89] While the imaging appearance is nonspecific to allow a preoperative diagnosis, one of their most

characteristic features on MRI is perhaps the intrinsic T1 hyperin-tensity of some tumors, presumably related to densely packed cells and a low water content (Figure 14).[88] As opposed to chondrosar-comas or chordomas, which are markedly hyperintense on T2, plasmacytomas are relatively isointense to gray matter due to high cellularity and lack a calcific matrix or areas of sequestered bone.[88,90] Plasmacytomas enhance avidly and homogeneously, which are also features of lymphoma, but the latter tends to have intermediate to low signal intensity on both T1 and T2-weighted sequences.[30]

Metastases

Metastases to the skull base occur in approximately 4% of cancer patients.[91] While various tumors metastasize to this region, in one literature review, the most common primaries in order of frequency were prostate and breast cancer, lymphoma, and lung cancer.[92] Most skull base metastases probably spread hematogenously, although seeding may also occur through the valveless Batson venous plexus, which connects the pelvic and thoracic venous systems with intracranial veins and sinuses.[92,93] Additionally, the skull base can be involved by direct extension of nasopharyngeal or sphenoid tumors or via perineural spread, commonly along branches of CN V.[94,95] Infiltration can lead to a distinct parasellar syndrome, with neuropathies frequently involving CNs III and V.[96] On MRI, osseous metastases are typically identified as hypointense geographic areas of marrow replacement on noncontrast T1-weighted sequences. Because marrow fat is normally hyperintense on both T1- and T2-weighted sequences, fat saturation is useful to visualize

FIGURE 18. *Epidermoid tumor.* **A**, *Sagittal noncontrast T1-weighted image shows an extra-axial lesion (white arrows) in the suprasellar region and anterior to the brain stem. Its signal intensity is slightly higher than that of CSF.* **B**, *Axial T2-weighted image shows mild heterogeneity within an otherwise cystic-appearing lesion.* **C**, *Axial FLAIR demonstrates heterogeneous signal with a so-called "dirty" appearance (black arrows).* **D**, *Axial diffusion-weighted image shows increased signal from the lesion (arrowheads).*

metastases after administration of intravenous contrast material (Figure 15). Diffusion-weighted imaging may improve detection of calvarial metastases by showing areas of increased marrow signal, with the exception of prostate cancer, which is primarily sclerotic.[97,98]

In contradistinction, pituitary metastases are relatively rare. They are most frequently secondary to lung and breast cancer (more than one-half of cases), followed by renal and colorectal cancer.[99] Pituitary metastasis present as a mass involving the pituitary stalk or gland, may have a waist at the diaphragma sellae, can extend cranially to involve the hypothalamus, and the majority show loss of the pituitary bright spot and avid contrast enhancement.[99] Their distinction from adenomas is difficult. While smooth expansion of the sella favors an adenoma, erosion of the sella or skull base does not necessarily indicate a metastasis, as macroadenomas can be large and infiltrative.[100] Edema along the optic tracts may be present but is a nonspecific finding that can be seen in a variety of tumors.[101]

FIGURE 19. *Ruptured dermoid tumor. Sagittal noncontrast T1 shows a predominantly hyperintense suprasellar mass (arrow). Hyperintense lipid material can be seen in the lateral and fourth ventricles, quadrigeminal and prepontine cisterns, and posterior fossa.*

CONGENITAL

Rathke Cleft Cyst

These are benign, true epithelial cysts believed to arise from remnants of Rathke's pouch due to incomplete obliteration of the embryonic cleft.[30] They are more common in females, with symptomatic patients usually presenting between ages 30 and 60, although they may be seen at any age.[30,102] While the majority of them are small, asymptomatic, and found incidentally (in up to 33% of pituitary glands at autopsy), they may occasionally grow and cause mass effect.[102,103] Their contents are almost always homogeneous, but their signal characteristics on MRI vary according to the presence of protein, mucopolysaccharides, and, rarely, hemorrhage.[104] They are located centrally or near centrally within the pituitary gland (typically without deviation of the stalk) between the pars distalis and the pars intermedia but may also have suprasellar extension (Figure 16).[18,102] While they are frequently hyperintense on T2-weighted images, lesions that are homogeneously T2 hypointense are highly suggestive of the diagnosis, as is the presence of a T1-hyperintense and T2-hypointense intracystic nodule (representing a mucinous mass with cholesterol and protein) (Figure 17).[103,105,106] Aside from intracystic nodules and epithelial rests, they do not have solid components, do not enhance with contrast material, and rarely calcify.[104] Rathke cleft cysts may rarely be complicated by infection, hemorrhage, or chemical meningitis.[107,108]
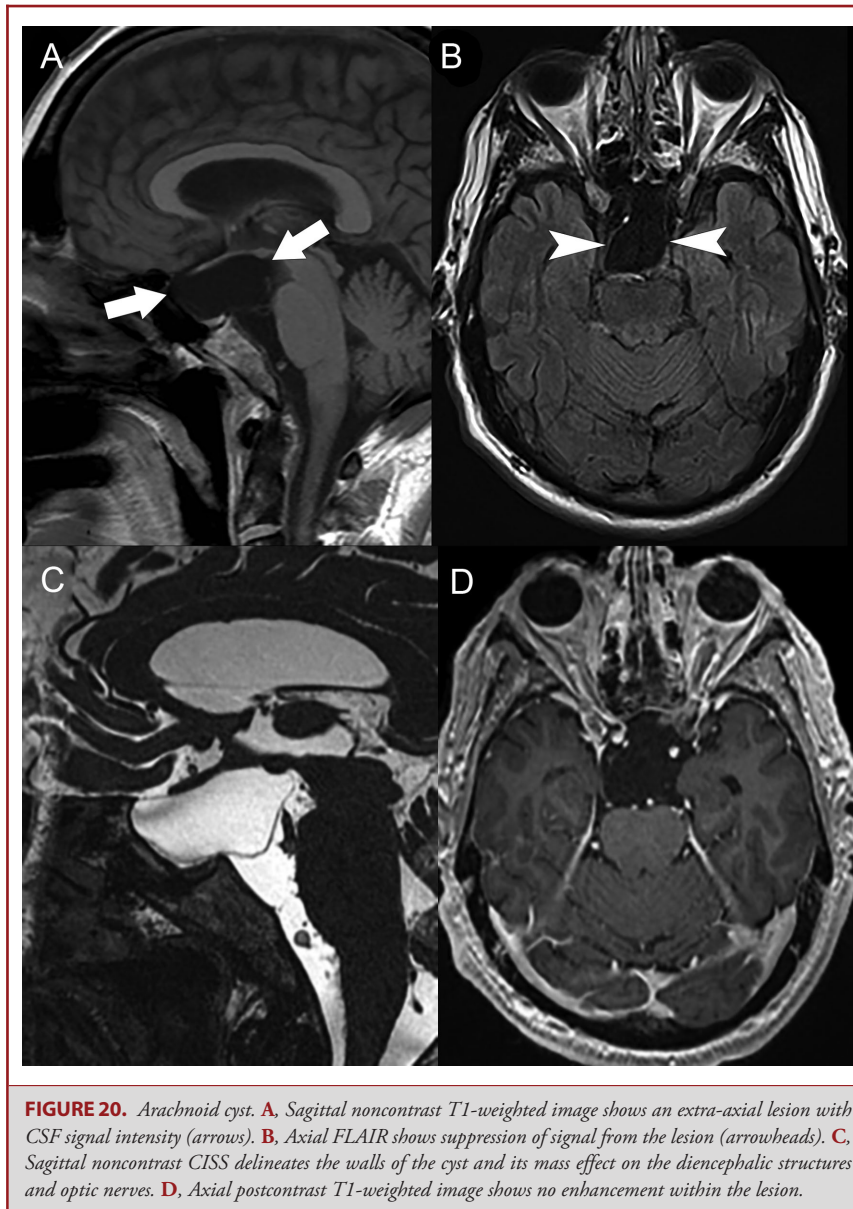
Dermoid and Epidermoid Tumor

Both of these nonneoplastic lesions develop from inclusion of ectodermal remnants during neural tube closure and differ histopathologically in that dermoids contain dermal appendages and epidermoids do not.[109,110] They both accumulate desquamated debris from their capsules and grow slowly.[109] Despite being congenital, they are infrequently found in children and usually manifest later in life.[109] Both are rare, but dermoids are less common.[108] Their location may vary, but dermoids are more commonly found midline while epidermoids tend to occur off-midline or asymmetrically to one side.[108,110] Between 40% and 50% of intracranial epidermoids occur in the cerebellopontine angles, 30% are parasellar, and 25% are primarily intraosseous with potential involvement of the subdural space.[111]

On CT, most epidermoids have low density that approaches CSF and may be difficult to distinguish from arachnoid cysts. Increased density in a minority of them may result from hemorrhage, increased protein, or saponification.[112,113] On MRI, their T1 and T2 signal intensities are usually close to those of CSF, but the lesion does not suppress on fluid-attenuated inversion recovery (FLAIR) sequences, on which it shows a "dirty" appearance (Figure 18).[114] Classically, they demonstrate very high ("light bulb bright") signal intensity on diffusion-weighted sequences, with ADC values that may not be as low as expected, probably from a combination of restricted diffusion and T2 shine-through effects.[114,115] Calcification is present in 10% of epidermoid tumors.[116] Dermoids tend to follow fat characteristics on CT and MRI but may be hypointense on T2 (Figure 19). Except for a thin peripheral rim in some, dermoids and epidermoids do not enhance.[116,117] Malignant transformation to squamous cell carcinoma is rare and can be seen in both lesions but is more common in epidermoids.[118]

Arachnoid Cyst

Arachnoid cysts are benign nonneoplastic structures filled with CSF and lined by arachnoid cells and collagen.[119] They are more common in males and have an imaging prevalence of 1% to 3%, with 75% found in children.[120,121] Between one-third and one-half are located in the middle cranial fossa, followed by the retrocerebellar region.[121,122] Growth is rare for incidentally found cysts and the majority are asymptomatic, although they occasionally may result in obstructive hydrocephalus, cranial neuropathies, seizures, or headaches.[121] Lack of or incomplete communication between the cyst and subarachnoid space is thought to be a factor in the development of mass effect and progressive symptoms.[123] While this has traditionally been assessed with CT cisternography, more recent studies have focused on the use of phase-contrast MRI to document jet-like flow within communicating arachnoid cysts or on the demonstration of cyst walls using SSFP sequences (Figure 20).[123-125] Arachnoid cysts are well-demarcated, expansile, and unilocular lesions without internal architecture, which often result in osseous remodeling.[83,126] Most arachnoid cysts follow CSF signal intensity on all MRI sequences

FIGURE 20. *Arachnoid cyst.* **A**, *Sagittal noncontrast T1-weighted image shows an extra-axial lesion with CSF signal intensity (arrows).* **B**, *Axial FLAIR shows suppression of signal from the lesion (arrowheads).* **C**, *Sagittal noncontrast CISS delineates the walls of the cyst and its mass effect on the diencephalic structures and optic nerves.* **D**, *Axial postcontrast T1-weighted image shows no enhancement within the lesion.*

and suppress on FLAIR, except for some that may contain increased proteins or hemorrhage.[126]
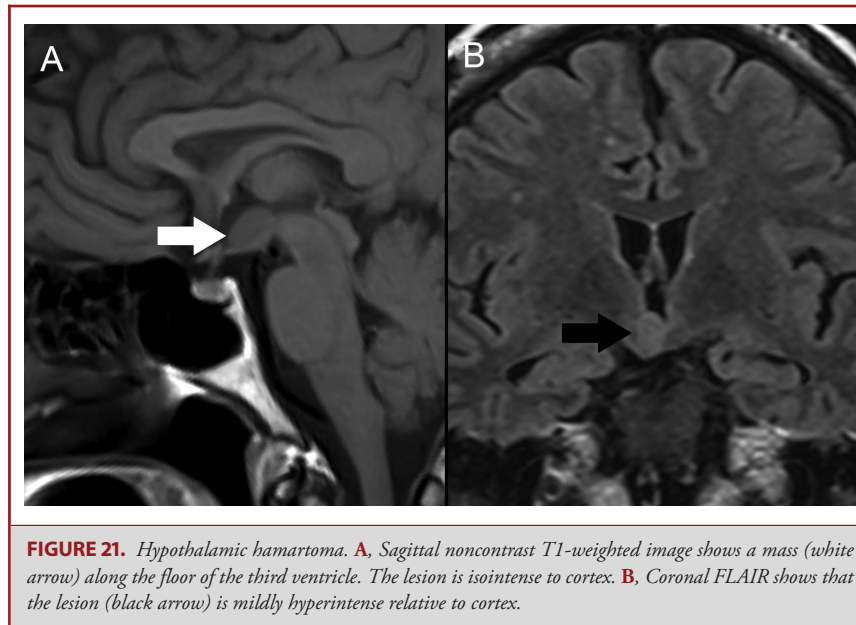
Hypothalamic Hamartoma

These are benign lesions consisting of neuronal and glial tissues that arise from the inferior hypothalamus or tuber cinereum.[127,128] They are classically associated with gelastic seizures, precocious puberty, and developmental delay, although there is considerable variability in their presentation.[129] Hamartomas can develop along the floor of the third ventricle or within the hypothalamus proper or be pedunculated, often with attachments to the mammillary bodies or tuber cinereum.[129,130] On

MRI, they do not strictly follow gray matter signal intensity, and most are mildly hyperintense on T2 (probably due to glial tissue) and iso- to hypointense on T1-weighted sequences (Figure 21).[128-130] Like normal brain parenchyma, hamartomas have a functional blood–brain barrier and should not show contrast enhancement.[130]

VASCULAR

Giant Aneurysm

Most aneurysms are thought to develop from a combination of hemodynamic stress and acquired or inherited factors (including

FIGURE 21. *Hypothalamic hamartoma.* **A***, Sagittal noncontrast T1-weighted image shows a mass (white arrow) along the floor of the third ventricle. The lesion is isointense to cortex.* **B***, Coronal FLAIR shows that the lesion (black arrow) is mildly hyperintense relative to cortex.*

connective tissue disorders) that result in progressive weakening of the parent vessel.[131] Giant aneurysms are greater than 25 mm in diameter and are rare but important lesions that may occur in the suprasellar or parasellar regions.[132] Their recognition is critical due to treatment implications and, most importantly, to avoid a catastrophic biopsy. Giant aneurysms can cause osseous erosion of the skull base and may occasionally extend to the parapharyngeal space, paranasal sinuses, or infratemporal fossa.[133] Their imaging characteristics may be misleading, with heterogeneous signal intensities and incomplete enhancement owing to thrombosis and blood at various stages. Areas of profound T2 hypointensity within a skull base mass may represent a vascular flow void, and the lesion should be carefully scrutinized to rule out an aneurysm. Pulsation artifact in the phase-encoding direction may be a useful clue when present (Figure 22).

INFLAMMATORY/GRANULOMATOUS

Sarcoidosis

Autopsy studies have found subclinical CNS involvement in 25% of patients with systemic sarcoidosis.[134,135] This can involve any part of the brain, meninges, cranial nerves, or calvarium, and its appearance is nonspecific, with leptomeningeal or pachymeningeal thickening and enhancement and/or cerebral or soft-tissue granulomata.[136] Infiltration of the pituitary gland and infundibulum/hypothalamus is rare and generally proportional to disease severity but can rarely occur in isolation (which may mimic the appearance of lymphocytic hypophysitis or Langerhans cell histiocytosis).[135] More commonly, hypothalamic/pituitary involvement is associated with nodular leptomeningeal basilar

enhancement.[135-137] As with other granulomatous infections, sarcoid lesions may be hypointense on T2-weighted images, but this finding is nonspecific (Figure 23).[137]

Lymphocytic Hypophysitis

Lymphocytic hypophysitis is an infiltrative autoimmune/inflammatory disorder that may affect the anterior or posterior pituitary gland or infundibulum and is characterized by variable degrees of pituitary dysfunction.[138] It is most commonly seen in pregnant or postpartum patients but has also been linked to a number of autoimmune conditions, including drug related (eg, ipilimumab).[139] Its imaging appearance is nonspecific and may be indistinguishable from other infiltrative processes such as Langerhans cell histiocytosis and may also be confused with primary or metastatic neoplasms. It usually leads to thickening and avid enhancement of the affected portions of the gland, sometimes with absence of the pituitary bright spot (Figure 24).[140] In some patients, a T2-hypointense area is seen in the parasellar region, which may suggest the diagnosis.[138]

CONCLUSION

The sellar and parasellar regions are relatively small areas of the skull base that harbor important neurovascular structures and feature complex anatomy. The pathology that can occur at these sites is varied, and some of the diseases may present with similar clinical and imaging characteristics. Knowledge of relevant neuroimaging features may assist in characterization of these lesions, delineation of their extent, and
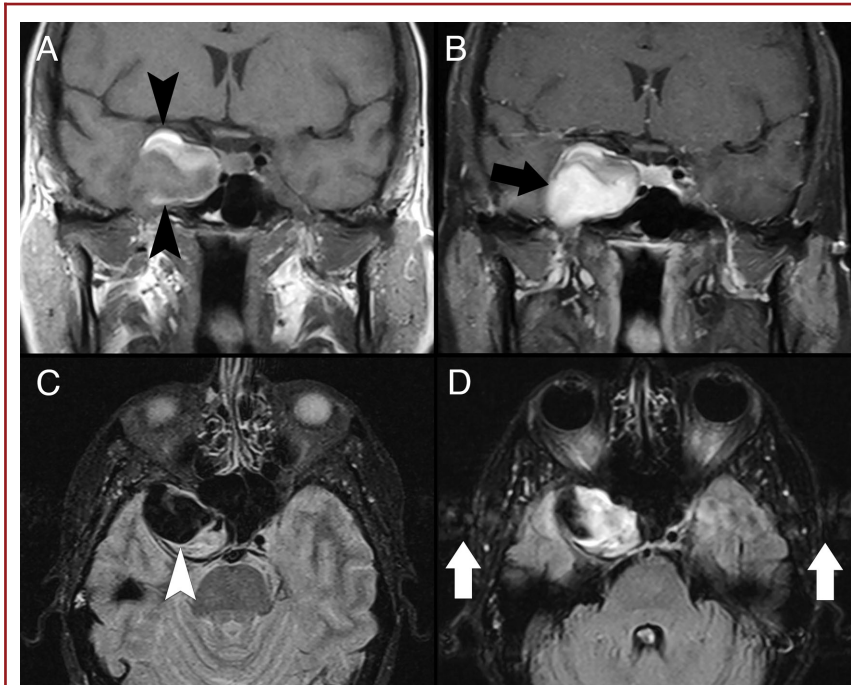
FIGURE 22. *Giant parasellar aneurysm.* **A**, *Coronal noncontrast T1-weighted image shows a partially thrombosed aneurysm (black arrowheads) along the right aspect of the sella and middle cranial fossa.* **B**, *Coronal postcontrast T1-weighted image shows enhancement of the nonthrombosed inferior portion of the aneurysm (black arrow).* **C**, *Axial T2-weighted image demonstrates a vascular flow void (white arrowhead) related to the perfused portion of the aneurysm.* **D**, *Axial FLAIR image shows the presence of pulsation artifact along the phase-encoding direction (white arrows).*
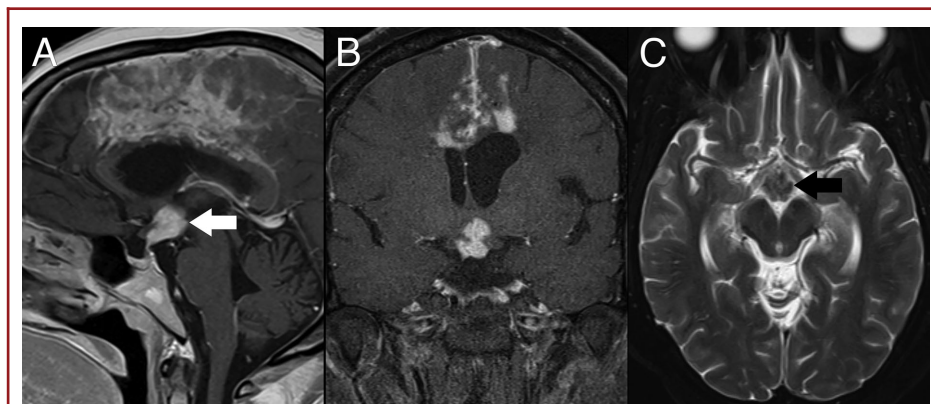
FIGURE 23. *Neurosarcoid.* **A**, *Sagittal postcontrast T1-weighted image shows enhancing tissue in the hypothalamus and along the upper pituitary infundibulum (white arrow) as well as leptomeningeal enhancement along the falx cerebri.* **B**, *Coronal postcontrast T1-weighted image shows that the lesion partially encases the prechiasmatic optic nerves. There is leptomeningeal enhancement along the falx cerebri and there are granulomas in the corpus callosum.* **C**, *Axial T2-weighted image shows the suprasellar sarcoid granuloma to be hypointense (black arrow).*
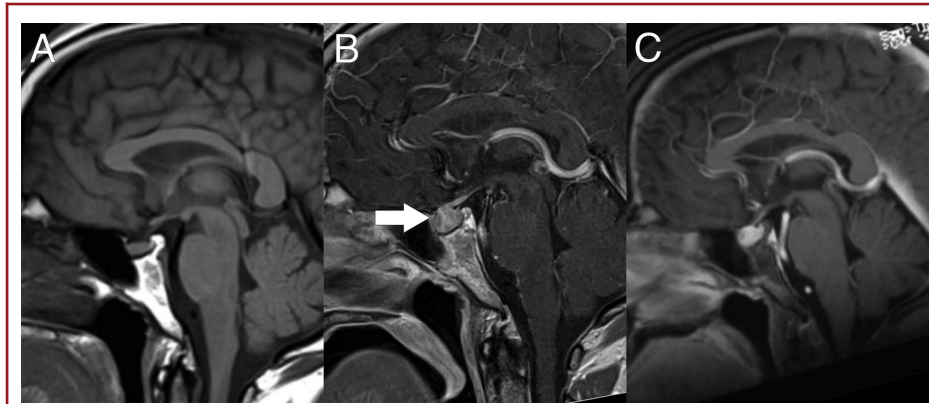
FIGURE 24. *Autoimmune hypophysitis in a patient with hypopituitarism following ipilimumab infusion for melanoma.* **A***, Baseline noncontrast sagittal T1-weighted image shows a normal configuration of the pituitary gland.* **B***, Sagittal postcontrast T1-weighted image 9 days after ipilimumab infusion shows enlargement and enhancement of the pituitary gland (arrow) and infundibulum.* **C***, Sagittal postcontrast T1-weighted image 5 days later shows decreased size and enhancement of these structures.*

awareness of potential mimics prior to diagnostic biopsy or resection.

Disclosure

The authors have no personal, financial, or institutional interest in any of the drugs, materials, or devices described in this article.

REFERENCES

1. Kollias SS, Ball WS, Prenger EC. Review of the embryologic development of the pituitary gland and report of a case of hypophyseal duplication detected by MRI. *Neuroradiology*. 1995;37(1):3-12.
2. Ikeda H, Suzuki J, Sasano N, Niizuma H. The development and morphogenesis of the human pituitary gland. *Anat Embryol (Berl)*. 1988;178(4):327-336.
3. Larkin S, Karavitaki N, Ansorge O. Rathke's cleft cyst. In: *Handbook of Clinical Neurology*. Vol 2. Elsevier, Cambridge, MA 02139, USA. 2014:255-269.
4. Solov'ev GS, Bogdanov AV, Panteleev SM, Yanin VL. Embryonic morphogenesis of the human pituitary. *Neurosci Behav Physiol*. 2008;38(8):829-833.
5. Patel CR, Fernandez-Miranda JC, Wang WH, Wang EW. Skull base anatomy. *Otolaryngol Clin North Am*. 2016;49(1):9-20.
6. Chavhan GB, Babyn PS, Jankharia BG, Cheng HL, Shroff MM. Steady-state MR imaging sequences: physics, classification, and clinical applications. *Radiographics*. 2008;28(4):1147-1160.
7. Xie T, Zhang XB, Yun H, Hu F, Yu Y, Gu Y. 3D-FIESTA MR images are useful in the evaluation of the endoscopic expanded endonasal approach for midline skull-base lesions. *Acta Neurochir (Wien)*. 2011;153(1):12-18.
8. Blitz AM, Macedo LL, Chonka ZD, et al. High-resolution CISS MR imaging with and without contrast for evaluation of the upper cranial nerves: segmental anatomy and selected pathologic conditions of the cisternal through extraforaminal segments. *Neuroimaging Clin N Am*. 2014;24(1):17-34.
9. Hayashi M, Chernov MF, Tamura N, et al. Usefulness of the advanced neuroimaging protocol based on plain and gadolinium-enhanced constructive interference in steady state images for gamma knife radiosurgery and planning microsurgical procedures for skull base tumors. *Acta Neurochir Suppl (Wien)*. 2013;116:167-178.
10. Fischbach F, Muller M, Bruhn H. Magnetic resonance imaging of the cranial nerves in the posterior fossa: a comparative study of t2-weighted spin-echo sequences at 1.5 and 3.0 tesla. *Acta Radiol*. 2008;49(3):358-363.
11. Furutani K, Harada M, Mawlan M, Nishitani H. Difference in enhancement between spin echo and 3-dimensional fast spoiled gradient recalled acquisition in steady state magnetic resonance imaging of brain metastasis at 3-T magnetic resonance imaging. *J Comput Assist Tomogr*. 2008;32(2):313-319.
12. Gao R, Isoda H, Tanaka T, et al. Dynamic gadolinium-enhanced MR imaging of pituitary adenomas: usefulness of sequential sagittal and coronal plane images. *Eur J Radiol*. 2001;39(3):139-146.
13. Friedman TC, Zuckerbraun E, Lee ML, Kabil MS, Shahinian H. Dynamic pituitary MRI has high sensitivity and specificity for the diagnosis of mild Cushing's syndrome and should be part of the initial workup. *Horm Metab Res*. 2007;39(6):451-456.
14. Sakamoto Y, Takahashi M, Korogi Y, Bussaka H, Ushio Y. Normal and abnormal pituitary glands: gadopentetate dimeglumine-enhanced MR imaging. *Radiology*. 1991;178(2):441-445.
15. Chabot JD, Chakraborty S, Imbarrato G, Dehdashti AR. Evaluation of outcomes after endoscopic endonasal surgery for large and giant pituitary macroadenoma: a retrospective review of 39 consecutive patients. *World Neurosurg*. 2015;84(4):978-988.
16. Ezzat S, Asa SL, Couldwell WT, et al. The prevalence of pituitary adenomas: a systematic review. *Cancer*. 2004;101(3):613-619.
17. Agustsson TT, Baldvinsdottir T, Jonasson JG, et al. The epidemiology of pituitary adenomas in Iceland, 1955-2012: a nationwide population-based study. *Eur J Endocrinol*. 2015;173(5):655-664.
18. Castillo M. Pituitary gland: development, normal appearances, and magnetic resonance imaging protocols. *TMRI*. 2005;16(4):259-268.
19. Miki Y, Matsuo M, Nishizawa S, et al. Pituitary adenomas and normal pituitary tissue: enhancement patterns on gadopentetate-enhanced MR imaging. *Radiology*. 1990;177(1):35-38.
20. Bonneville JF, Bonneville F, Cattin F. Magnetic resonance imaging of pituitary adenomas. *Eur Radiol*. 2005;15(3):543-548.
21. Hagiwara A, Inoue Y, Wakasa K, Haba T, Tashiro T, Miyamoto T. Comparison of growth hormone-producing and non-growth hormone-producing pituitary adenomas: imaging characteristics and pathologic correlation. *Radiology*. 2003;228(2):533-538.
22. Potorac I, Petrossians P, Daly AF, et al. Pituitary MRI characteristics in 297 acromegaly patients based on T2-weighted sequences. *Endocr Relat Cancer*. 2015;22(2):169-177.
23. Ahmadi J, North CM, Segall HD, Zee CS, Weiss MH. Cavernous sinus invasion by pituitary adenomas. *Am J Roentgenol*. 1986;146(2):257-262.
24. Cottier JP, Destrieux C, Brunereau L, et al. Cavernous sinus invasion by pituitary adenoma: MR imaging. *Radiology*. 2000;215(2):463-469.
25. Vieira JO, Jr, Cukiert A, Liberman B. Evaluation of magnetic resonance imaging criteria for cavernous sinus invasion in patients with pituitary adenomas:

logistic regression analysis and correlation with surgical findings. *Surg Neurol.* 2006;65(2):130-135; discussion 135.

26. Inagawa H, Ishizawa K, Mitsuhashi T, et al. Giant invasive pituitary adenoma extending into the sphenoid sinus and nasopharynx: report of a case with intra-operative cytologic diagnosis. *Acta Cytol.* 2005;49(4):452-456.

27. Briet C, Salenave S, Chanson P. Pituitary apoplexy. *Endocrinol Metab Clin North Am.* 2015;44(1):199-209.

28. Oldfield EH, Merrill MJ. Apoplexy of pituitary adenomas: the perfect storm. *J Neurosurg.* 2015;122(6):1444-1449.

29. Azizyan A, Miller JM, Azzam RI, et al. Spontaneous retroclival hematoma in pituitary apoplexy: case series. *J Neurosurg.* 2015;123(3):808-812.

30. Huang BY, Castillo M. Nonadenomatous tumors of the pituitary and sella turcica. *TMRI.* 2005;16(4):289-299.

31. Dolecek TA, Dressler EV, Thakkar JP, Liu M, Al-Qaisi A, Villano JL. Epidemiology of meningiomas post-Public Law 107-206: the benign brain tumor cancer registries amendment act. *Cancer.* 2015;121(14):2400-2410.

32. Zhou P, Ma W, Yin S, Li Y, Jiang S. Three risk factors for WHO grade II and III meningiomas: a study of 1737 cases from a single center. *Neurol India.* 2013;61(1):40-44.

33. Bhat AR, Wani MA, Kirmani AR, Ramzan AU. Histological-subtypes and anatomical location correlated in meningeal brain tumors (meningiomas). *J Neurosci Rural Pract.* 2014;5(3):244-249.

34. Fathi AR, Roelcke U. Meningioma. *Curr Neurol Neurosci Rep.* 2013;13(4):337.

35. Barshes N, Demopoulos A, Engelhard HH. Anatomy and physi-ology of the leptomeninges and CSF space. *Cancer Treat Res.* 2005;125:1-16.

36. Schick U, Hassler W. Surgical management of tuberculum sellae meningiomas: involvement of the optic canal and visual outcome. *J Neurol Neurosurg Psychiatry.* 2005;76(7):977-983.

37. DeMonte F. Surgical treatment of anterior basal meningiomas. *J Neurooncol.* 1996;29(3):239-248.

38. Nanda A, Konar SK, Maiti TK, Bir SC, Guthikonda B. Stratification of predictive factors to assess resectability and surgical outcome in clinoidal menin-gioma. *Clin Neurol Neurosurg.* 2016;142:31-37.

39. Parizel PM, Carpentier K, Van Marck V, et al. Pneumosinus dilatans in anterior skull base meningiomas. *Neuroradiology.* 2013;55(3):307-311.

40. Pieper DR, Al-Mefty O, Hanada Y, Buechner D. Hyperostosis associated with meningioma of the cranial base: secondary changes or tumor invasion. *Neuro-surgery.* 1999;44(4):742-746; discussion 746-747.

41. Rokni-Yazdi H, Sotoudeh H. Prevalence of "dural tail sign" in patients with different intracranial pathologies. *Eur J Radiol.* 2006;60(1):42-45.

42. Goldsher D, Litt AW, Pinto RS, Bannon KR, Kricheff II. Dural "tail" associated with meningiomas on Gd-DTPA-enhanced MR images: character-istics, differential diagnostic value, and possible implications for treatment. *Radiology.* 1990;176(2):447-450.

43. Schwyzer L, Berberat J, Remonda L, Roelcke U. Susceptibility changes in meningiomas influence the apparent diffusion coefficient in diffusion-weighted MRI. *J Neuroradiol.* 2015;42(6):332-337.

44. Fernandez-Miranda JC, Gardner PA, Snyderman CH, et al. Craniopharyn-gioma: a pathologic, clinical, and surgical review. *Head Neck.* 2012;34(7):1036-1044.

45. Zada G, Lin N, Ojerholm E, Ramkissoon S, Laws ER. Craniopharyngioma and other cystic epithelial lesions of the sellar region: a review of clinical, imaging, and histopathological relationships. *Neurosurg Focus.* 2010;28(4):E4.

46. Muller HL. Craniopharyngioma. *Endocr Rev.* 2014;35(3):513-543.

47. Bunin GR, Surawicz TS, Witman PA, Preston-Martin S, Davis F, Bruner JM. The descriptive epidemiology of craniopharyngioma. *J Neurosurg.* 1998;89(4):547-551.

48. Ostrom QT, de Blank PM, Kruchko C, et al. Alex's Lemonade Stand Foundation: infant and childhood primary brain and central nervous system tumors diagnosed in the United States in 2007-2011. *Neuro oncol.* 2015;16(suppl 10):x1-x36.

49. Lee HJ, Wu CC, Wu HM, et al. Pretreatment diagnosis of suprasellar papillary craniopharyngioma and germ cell tumors of adult patients. *Am J Neuroradiol.* 2015;36(3):508-517.

50. Almefty K, Pravdenkova S, Colli BO, Al-Mefty O, Gokden M. Chordoma and chondrosarcoma: similar, but quite different, skull base tumors. *Cancer.* 2007;110(11):2457-2467.

51. Fernandez-Miranda JC, Gardner PA, Snyderman CH, et al. Clival chordomas: a pathological, surgical, and radiotherapeutic review. *Head Neck.* 2014;36(6):892-906.

52. Jahangiri A, Jian B, Miller L, El-Sayed IH, Aghi MK. Skull base chordomas: clinical features, prognostic factors, and therapeutics. *Neurosurg Clin N Am.* 2013;24(1):79-88.

53. Erdem E, Angtuaco EC, Van Hemert R, Park JS, Al-Mefty O. Comprehensive review of intracranial chordoma. *Radiographics.* 2003;23(4):995-1009.

54. Sze G, Uichanco LS, 3rd, Brant-Zawadzki MN, et al. Chordomas: MR imaging. *Radiology.* 1988;166(1 Pt 1):187-191.

55. Meyers SP, Jr Hirsch WL, Curtin HD, Barnes L, Sekhar LN, Sen C. Chordomas of the skull base: MR features. *Am J Neuroradiol.* 1992;13(6):1627-1636.

56. Choi D, Gleeson M. Surgery for chordomas of the craniocervical junction: lessons learned. *Skull Base.* 2010;20(1):41-45.

57. Van Gompel JJ, Janus JR. Chordoma and chondrosarcoma. *Otolaryngol Clin North Am.* 2015;48(3):501-514.

58. Bloch O, Parsa AT. Skull base chondrosarcoma: evidence-based treatment paradigms. *Neurosurg Clin N Am.* 2013;24(1):89-96.

59. Aprile I, Scott CA, Cervesato D, Beltrami CA, Meo A, Fabris G. Two rare lumbar tumours with unusual MRI characteristics. *Neuroradiology.* 2000;42(6):458-461.

60. Bloch OG, Jian BJ, Yang I, et al. Cranial chondrosarcoma and recurrence. *Skull Base.* 2010;20(3):149-156.

61. Lustig LR, Sciubba J, Holliday MJ. Chondrosarcomas of the skull base and temporal bone. *J Laryngol Otol.* 2007;121(8):725-735.

62. Lee YY, Van Tassel P. Craniofacial chondrosarcomas: imaging findings in 15 untreated cases. *Am J Neuroradiol.* 1989;10(1):165-170.

63. Yeom KW, Lober RM, Mobley BC, et al. Diffusion-weighted MRI: distinction of skull base chordoma from chondrosarcoma. *Am J Neuroradiol.* 2013;34(5):1056-1061, S1051.

64. Chowdhury FH, Haque MR, Kawsar KA, Sarker MH, Hasan M, Goel AH. Intracranial nonvestibular neurinomas: young neurosurgeons' experience. *J Neurosci Rural Pract.* 2014;5(3):231-243.

65. MacNally SP, Rutherford SA, Ramsden RT, Evans DG, King AT. Trigeminal schwannomas. *Br J Neurosurg.* 2008;22(6):729-738.

66. Zhang L, Yang Y, Xu S, Wang J, Liu Y, Zhu S. Trigeminal schwannomas: a report of 42 cases and review of the relevant surgical approaches. *Clin Neurol Neurosurg.* 2009;111(3):261-269.

67. Liu XD, Xu QW, Che XM, Yang DL. Trigeminal neurinomas: clinical features and surgical experience in 84 patients. *Neurosurg Rev.* 2009;32(4):435-444.

68. Buhl R, Barth H, Hugo HH, Mautner VF, Mehdorn HM. Intracranial and spinal melanotic schwannoma in the same patient. *J Neurooncol.* 2004;68(3):249-254.

69. Dahlen RT, Johnson CE, Harnsberger HR, et al. CT and MR imaging characteristics of intravestibular lipoma. *Am J Neuroradiol.* 2002;23(8):1413-1417.

70. Fried I, Tabori U, Tihan T, Reginald A, Bouffet E. Optic pathway gliomas: a review. *CNS Oncol.* 2013;2(2):143-159.

71. Dutton JJ. Gliomas of the anterior visual pathway. *Surv Ophthalmol.* 1994;38(5):427-452.

72. Kornreich L, Blaser S, Schwarz M, et al. Optic pathway glioma: correlation of imaging findings with the presence of neurofibromatosis. *Am J Neuroradiol.* 2001;22(10):1963-1969.

73. Shamji MF, Benoit BG. Syndromic and sporadic pediatric optic pathway gliomas: review of clinical and histopathological differences and treatment impli-cations. *Neurosurg Focus.* 2007;23(5):E3.

74. Pepin SM, Lessell S. Anterior visual pathway gliomas: the last 30 years. *Semin Ophthalmol.* 2006;21(3):117-124.

75. Della Puppa A, Rustemi O, Gioffre G. The rare event of optic-chiasmatic hemor-rhagic low grade glioma in adulthood. Considerations on treatment strategy. *Neurol Sci.* 2014;35(4):623-625.

76. Echevarria ME, Fangusaro J, Goldman S. Pediatric central nervous system germ cell tumors: a review. *Oncologist.* 2008;13(6):690-699.

77. Poynter JN, Fonstad R, Tolar J, Spector LG, Ross JA. Incidence of intracranial germ cell tumors by race in the United States, 1992-2010. *J Neurooncol.* 2014;120(2):381-388.

78. Packer RJ, Cohen BH, Cooney K. Intracranial germ cell tumors. *Oncologist.* 2000;5(4):312-320.

79. Villano JL, Propp JM, Porter KR, et al. Malignant pineal germ-cell tumors: an analysis of cases from three tumor registries. *Neuro oncol.* 2008;10(2):121-130.

80. Jennings MT, Gelman R, Hochberg F. Intracranial germ-cell tumors: natural history and pathogenesis. *J Neurosurg.* 1985;63(2):155-167.

81. Kim DI, Yoon PH, Ryu YH, Jeon P, Hwang GJ. MRI of germinomas arising from the basal ganglia and thalamus. *Neuroradiology.* 1998;40(8):507-511.

82. Ozelame RV, Shroff M, Wood B, et al. Basal ganglia germinoma in children with associated ipsilateral cerebral and brain stem hemiatrophy. *Pediatr Radiol.* 2006;36(4):325-330.

83. Borja MJ, Plaza MJ, Altman N, Saigal G. Conventional and advanced MRI features of pediatric intracranial tumors: supratentorial tumors. *Am J Roentgenol.* 2013;200(5):W483-503.

84. Kanagaki M, Miki Y, Takahashi JA, et al. MRI and CT findings of neurohy-pophyseal germinoma. *Eur J Radiol.* 2004;49(3):204-211.

85. Ogiwara H, Tsutsumi Y, Matsuoka K, Kiyotani C, Terashima K, Morota N. Apparent diffusion coefficient of intracranial germ cell tumors. *J Neurooncol.* 2015;121(3):565-571.

86. Cerase A, Tarantino A, Gozzetti A, et al. Intracranial involvement in plasmacytomas and multiple myeloma: a pictorial essay. *Neuroradiology.* 2008;50(8):665-674.

87. Dimopoulos MA, Moulopoulos LA, Maniatis A, Alexanian R. Solitary plasmacytoma of bone and asymptomatic multiple myeloma. *Blood.* 2000;96(6):2037-2044.

88. Wein RO, Popat SR, Doerr TD, Dutcher PO. Plasma cell tumors of the skull base: four case reports and literature review. *Skull Base.* 2002;12(2):77-86.

89. Gangadhar K, Santhosh D. Radiopathological evaluation of primary malignant skull tumors: a review. *Clin Neurol Neurosurg.* 2012;114(7):833-839.

90. Agarwal A. Neuroimaging of plasmacytoma. A pictorial review. *Neuroradiol J.* 2014;27(4):431-437.

91. Greenberg HS, Deck MD, Vikram B, Chu FC, Posner JB. Metastasis to the base of the skull: clinical findings in 43 patients. *Neurology.* 1981;31(5):530-537.

92. Laigle-Donadey F, Taillibert S, Martin-Duverneuil N, Hildebrand J, Delattre JY. Skull-base metastases. *J Neurooncol.* 2005;75(1):63-69.

93. Pearce JM. The craniospinal venous system. *Eur Neurol.* 2006;56(2):136-138.

94. Razek AA, Castillo M. Imaging lesions of the cavernous sinus. *Am J Neuroradiol.* 2009;30(3):444-452.

95. Roh JL, Sung MW, Kim KH, et al. Nasopharyngeal carcinoma with skull base invasion: a necessity of staging subdivision. *Am J Otolaryngol.* 2004;25(1):26-32.

96. Johnston JL. Parasellar syndromes. *Curr Neurol Neurosci Rep.* 2002;2(5):423-431.

97. Ginat DT, Mangla R, Yeaney G, Ekholm S. Diffusion-weighted imaging of skull lesions. *J Neurol Surg B Skull Base.* 2014;75(3):204-213.

98. Nemeth AJ, Henson JW, Mullins ME, Gonzalez RG, Schaefer PW. Improved detection of skull metastasis with diffusion-weighted MR imaging. *Am J Neuro-radiol.* 2007;28(6):1088-1092.

99. Habu M, Tokimura H, Hirano H, et al. Pituitary metastases: current practice in Japan. *J Neurosurg.* 2015;123(4):998-1007.

100. Shrivastava RK, Arginteanu MS, King WA, Post KD. Giant prolactinomas: clinical management and long-term follow up. *J Neurosurg.* 2002;97(2):299-306.

101. Saeki N, Uchino Y, Murai H, et al. MR imaging study of edema-like change along the optic tract in patients with pituitary region tumors. *Am J Neuroradiol.* 2003;24(3):336-342.

102. Han SJ, Rolston JD, Jahangiri A, Aghi MK. Rathke's cleft cysts: review of natural history and surgical outcomes. *J Neurooncol.* 2014;117(2):197-203.

103. Byun WM, Kim OL, Kim D. MR imaging findings of Rathke's cleft cysts: significance of intracystic nodules. *Am J Neuroradiol.* 2000;21(3):485-488.

104. Nishioka H, Haraoka J, Izawa H, Ikeda Y. Magnetic resonance imaging, clinical manifestations, and management of Rathke's cleft cyst. *Clin Endocrinol (Oxf).* 2006;64(2):184-188.

105. Bonneville F, Chiras J, Cattin F, Bonneville JF. T2 hypointense signal of rathke cleft cyst. *Am J Neuroradiol.* 2007;28(3):397.

106. Park M, Lee SK, Choi J, et al. Differentiation between cystic pituitary adenomas and Rathke Cleft Cysts: a diagnostic model using MRI. *Am J Neuroradiol.* 2015;36(10):1866-1873.

107. Chaiban JT, Abdelmannan D, Cohen M, Selman WR, Arafah BM. Rathke cleft cyst apoplexy: a newly characterized distinct clinical entity. *J Neurosurg.* 2011;114(2):318-324.

108. Hess CP, Dillon WP. Imaging the pituitary and parasellar region. *Neurosurg Clin N Am.* 2012;23(4):529-542.

109. Caldarelli M, Massimi L, Kondageski C, Di Rocco C. Intracranial midline dermoid and epidermoid cysts in children. *J Neurosurg.* 2004;100(5 suppl Pediatrics):473-480.

110. Orakcioglu B, Halatsch ME, Fortunati M, Unterberg A, Yonekawa Y. Intracranial dermoid cysts: variations of radiological and clinical features. *Acta Neurochir (Wien).* 2008;150(12):1227-1234; discussion 1234.

111. Nagasawa DT, Choy W, Spasic M, et al. An analysis of intracranial epidermoid tumors with malignant transformation: treatment and outcomes. *Clin Neurol Neurosurg.* 2013;115(7):1071-1078.

112. Timmer FA, Sluzewski M, Treskes M, van Rooij WJ, Teepen JL, Wijnalda D. Chemical analysis of an epidermoid cyst with unusual CT and MR characteristics. *Am J Neuroradiol.* 1998;19(6):1111-1112.

113. Brown JY, Morokoff AP, Mitchell PJ, Gonzales MF. Unusual imaging appearance of an intracranial dermoid cyst. *Am J Neuroradiol.* 2001;22(10):1970-1972.

114. Hakyemez B, Aksoy U, Yildiz H, Ergin N. Intracranial epidermoid cysts: diffusion-weighted, FLAIR and conventional MR findings. *Eur J Radiol.* 2005;54(2):214-220.

115. Santhosh K, Thomas B, Radhakrishnan VV, et al. Diffusion tensor and tensor metrics imaging in intracranial epidermoid cysts. *JMRI.* 2009;29(4):967-970.

116. Nagasawa D, Yew A, Safaee M, et al. Clinical characteristics and diagnostic imaging of epidermoid tumors. *J Clin Neurosci.* 2011;18(9):1158-1162.

117. Ren X, Lin S, Wang Z, et al. Clinical, radiological, and pathological features of 24 atypical intracranial epidermoid cysts. *J Neurosurg.* 2012;116(3):611-621.

118. Hamlat A, Hua ZF, Saikali S, et al. Malignant transformation of intra-cranial epithelial cysts: systematic article review. *J Neurooncol.* 2005;74(2):187-194.

119. Rengachary SS, Watanabe I. Ultrastructure and pathogenesis of intracranial arachnoid cysts. *J Neuropathol Exp Neurol.* 1981;40(1):61-83.

120. Al-Holou WN, Yew AY, Boomsaad ZE, Garton HJ, Muraszko KM, Maher CO. Prevalence and natural history of arachnoid cysts in children. *J Neurosurg. Pediat.* 2010;5(6):578-585.

121. Al-Holou WN, Terman S, Kilburg C, Garton HJ, Muraszko KM, Maher CO. Prevalence and natural history of arachnoid cysts in adults. *J Neurosurg.* 2013;118(2):222-231.

122. Cincu R, Agrawal A, Eiras J. Intracranial arachnoid cysts: current concepts and treatment alternatives. *Clin Neurol Neurosurg.* 2007;109(10):837-843.

123. Yildiz H, Erdogan C, Yalcin R, et al. Evaluation of communication between intracranial arachnoid cysts and cisterns with phase-contrast cine MR imaging. *Am J Neuroradiol.* 2005;26(1):145-151.

124. Algin O, Hakyemez B, Gokalp G, Korfali E, Parlak M. Phase-contrast cine MRI versus MR cisternography on the evaluation of the communication between intraventricular arachnoid cysts and neighbouring cerebrospinal fluid spaces. *Neuroradiology.* 2009;51(5):305-312.

125. Awaji M, Okamoto K, Nishiyama K. Magnetic resonance cisternography for preoperative evaluation of arachnoid cysts. *Neuroradiology.* 2007;49(9):721-726.

126. Osborn AG, Preece MT. Intracranial cysts: radiologic-pathologic correlation and imaging approach. *Radiology.* 2006;239(3):650-664.

127. Maixner W. Hypothalamic hamartomas—clinical, neuropathological and surgical aspects. *Childs Nerv Syst.* 2006;22(8):867-873.

128. Amstutz DR, Coons SW, Kerrigan JF, Rekate HL, Heiserman JE. Hypothalamic hamartomas: correlation of MR imaging and spectroscopic findings with tumor glial content. *Am J Neuroradiol.* 2006;27(4):794-798.

129. Mittal S, Mittal M, Montes JL, Farmer JP, Andermann F. Hypothalamic hamartomas. Part 1. Clinical, neuroimaging, and neurophysiological characteristics. *Neurosurg Focus.* 2013;34(6):E6.

130. Arita K, Ikawa F, Kurisu K, et al. The relationship between magnetic resonance imaging findings and clinical manifestations of hypothalamic hamartoma. *J Neurosurg.* 1999;91(2):212-220.

131. Bonneville F, Sourour N, Biondi A. Intracranial aneurysms: an overview. *Neuroimaging Clin N Am.* 2006;16(3):371-382, vii.

132. Choi IS, David C. Giant intracranial aneurysms: development, clinical presentation and treatment. *Eur J Radiol.* 2003;46(3):178-194.

133. Fisher A, Som PM, Mosesson RE, Lidov M, Liu TH. Giant intracranial aneurysms with skull base erosion and extracranial masses: CT and MR findings. *J Comput Assist Tomogr.* 1994;18(6):939-942.

134. Pawate S, Moses H, Sriram S. Presentations and outcomes of neurosarcoidosis: a study of 54 cases. *QJM*. 2009;102(7):449-460.

135. Langrand C, Bihan H, Raverot G, et al. Hypothalamo-pituitary sarcoidosis: a multicenter study of 24 patients. *QJM*. 2012;105(10):981-995.

136. Smith JK, Matheus MG, Castillo M. Imaging manifestations of neurosarcoidosis. *Am J Roentgenol*. 2004;182(2):289-295.

137. Shah R, Roberson GH, Cure JK. Correlation of MR imaging findings and clinical manifestations in neurosarcoidosis. *Am J Neuroradiol*. 2009;30(5):953-961.

138. Nakata Y, Sato N, Masumoto T, et al. Parasellar T2 dark sign on MR imaging in patients with lymphocytic hypophysitis. *Am J Neuroradiol*. 2010;31(10):1944-1950.

139. Araujo PB, Coelho MC, Arruda M, Gadelha MR, Neto LV. Ipilimumab-induced hypophysitis: review of the literature. *J Endocrinol Invest*. 2015;38(11):1159-1166.

140. Carpinteri R, Patelli I, Casanueva FF, Giustina A. Pituitary tumours: inflammatory and granulomatous expansive lesions of the pituitary. *Best Pract Res Clin Endocrinol Metab*. 2009;23(5):639-650.